Level scheme of ^{153}Sm obtained from the ^{152}Sm(n_{th}, γ) reaction using a γ-γ coincidence spectrometer

Nguyen Ngoc Anh,[1,*] Nguyen Quang Hung,[2,†] Nguyen Xuan Hai,[1,‡] Pham Dinh Khang,[3] A. M. Sukhovoj,[4] L. V. Mitsyna,[4] Ho Huu Thang,[1] and Le Hong Khiem[5,6]

[1]*Dalat Nuclear Research Institute, Vietnam Atomic Energy Institute, 01 Nguyen Tu Luc, Dalat City, Vietnam*
[2]*Institute of Fundamental and Applied Sciences, Duy Tan University, Ho Chi Minh City 700000, Vietnam*
[3]*Hanoi University of Science and Technology, 01 Dai Co Viet, Hanoi City, Vietnam*
[4]*Joint Institute for Nuclear Research, Dubna, Russia*
[5]*Institute of Physics, Vietnam Academy of Science and Technology, Hanoi City, Vietnam*
[6]*Graduate University of Science and Technology, Vietnam Academy of Science and Technology, Hanoi City, Vietnam*

(Received 18 February 2019; revised manuscript received 19 June 2019; published 15 August 2019)

The level scheme of the compound ^{153}Sm nucleus formed via the ^{152}Sm(n_{th}, γ) reaction is studied by using a γ-γ coincidence spectrometer at Dalat Nuclear Research Institute, Vietnam. All the γ cascades, which correspond to the decays from the compound state to 12 final levels of 0 ($\frac{3}{2}^+$), 7.535 ($\frac{5}{2}^+$), 35.844 ($\frac{3}{2}^-$), 90.875 ($\frac{5}{2}^-$), 126.412 ($\frac{1}{2}^-$), 127.298 ($\frac{3}{2}^-$), 182.902 ($\frac{5}{2}^-$), 321.113 ($\frac{3}{2}^+$), 404.129 ($\frac{1}{2}^-$), 405.470 ($\frac{3}{2}^-$), 414.924 ($\frac{1}{2}^+$), and 481.088 ($\frac{3}{2}^+$) keV, have been measured. A total number of 386 cascades corresponding to 576 γ transitions has been detected. Among these cascades, 103 primary γ transitions together with their corresponding intermediate levels and 299 secondary transitions have been determined. In addition, 29 primary γ transitions, 42 intermediate levels, and 8 secondary transitions have been found to be the same as those extracted from the Evaluated Nuclear Structure Data File (ENSDF) data. The remaining 74 primary γ transitions, 61 intermediate levels, and 291 secondary transitions are therefore considered as new data. In particular, based on an assumption that most of the transitions are dipole, we have tentatively assigned the unique spin value of $\frac{3}{2}\hbar$ for 53 observed intermediate levels corresponding to the cascades from the compound state to the final levels of 7.535 ($\frac{5}{2}^+$), 90.875 ($\frac{5}{2}^-$), and 182.902 ($\frac{5}{2}^-$) keV, whereas the remaining levels are assigned with the spin values in the range of [$\frac{1}{2}$, $\frac{3}{2}$]$\hbar$. Moreover, the total and partial (for the spin range of [$\frac{1}{2}$, $\frac{3}{2}$]$\hbar$) cumulative numbers of levels have been constructed by combining the ENSDF data with the new data obtained in the present experiment. Comparison between these new cumulative curves and those extracted from the nuclear level density (NLD) data, which are obtained using the Oslo method, shows that the maximum excitation energy E_{max}, defined as the energy threshold below which most of the excited levels are observed, is extended to about 1.2 and 1.8 MeV for the total and partial NLD data, respectively. These values of E_{max} are higher than those obtained by using the present ENSDF data, which are around 1 MeV. The new cumulative curves have also been compared with different phenomenological and microscopic NLD models, and the recent exact pairing plus independent-particle model at finite temperature (EP+IPM), in which no fitting parameter has been employed, is found to be the best-fit one. The present findings provide updated information on the nuclear level structure and make a step toward the completed level schemes of excited compound nuclei.

DOI: 10.1103/PhysRevC.100.024324

I. INTRODUCTION

The energy-level properties of excited nuclei (called the nuclear level scheme), which include the level energies, spins, parities, and γ rays associated with the excited levels, are important for the study of nuclear structure physics, nuclear reactions, and nuclear astrophysics. The level schemes of nuclei in the mass region $A \approx 150$–154 are of particular interest because the nuclear deformation in this region was predicted to change drastically with only slight variations of A [1,2]. Nuclei in this mass region are also called transitional nuclei. For example, ^{150}Sm and ^{152}Sm have very different level schemes as the former has vibrational and/or quasivibrational characteristics, whereas the latter follows the rotational ones [3]. Similarly, the level spectrum of ^{152}Sm shows both rotational and vibrational behaviors, whereas that of ^{154}Sm exhibits the strong rotational properties, indicating that this nucleus is strongly deformed [4]. Moreover, two odd nuclei, ^{151}Sm and ^{153}Sm, which fall, respectively, between the two sets (^{150}Sm, ^{152}Sm) and (^{152}Sm, ^{154}Sm), are expected to be affected by the interplay between the rotational and vibrational bands [5]. Therefore, the level schemes of ^{151,153}Sm odd nuclei have been an interesting subject for many experimental

*ngocanh8999@gmail.com
†nguyenquanghung5@duytan.edu.vn
‡xuannguyennri@gmail.com

and theoretical studies. The present paper focuses on the experimental study of the level scheme of ^{153}Sm by using the thermal neutron-capture reaction.

The level scheme of ^{153}Sm has been studied using different nuclear reactions and techniques [6] and all the experimental data have been compiled in the Evaluated Nuclear Structure Data File (ENSDF) library [7]. For instance, the level scheme of ^{153}Sm at the low-energy region (below 1.53 MeV) was studied using the β^- decay of ^{153}Pm as well as the decay from the isomeric state of ^{153}Sm to its ground state [8–11]. These experiments detected in total 25 excited levels, 17 of which have the unique spin values within the interval of $[\frac{1}{2}, \frac{9}{2}]\hbar$. The high-spin part in the level scheme of ^{153}Sm was measured by using the heavy-ion capture reactions, in which 28 excited levels, 25 of which have the unique spin values falling into the range of $[\frac{11}{2}, \frac{41}{2}]\hbar$, were reported [2,12,13]. However, the above experiments have not covered the excited levels whose energy and spin are in the regions of [1.5, 4.0] MeV and $[\frac{1}{2}, \frac{3}{2}]\hbar$, respectively. In these regions, several transfer reactions such as $^{151}(t, p)$ [14], ^{152}Sm(d, p) [15–17],^{154}Sm(d, t) [5,16,17], ^{154}Sm(p, d) [17,18], ^{152}Sm$(\alpha, {}^3$He$)$ [19], ^{154}Sm$(^3$He$, \alpha)$ [17], and ^{154}Eu(t, α) [20] have been employed and a considerable number of excited levels of ^{153}Sm within the spin range of $[\frac{1}{2}, \frac{11}{2}]\hbar$ have been explored. Most important, by using the ^{152}Sm(d, p) reaction, 132 excited levels below 3.929 MeV and 56 excited levels below 1.991 MeV in the level scheme of ^{153}Sm have been deduced in Refs. [15] and [16], respectively. Although the data reported in Refs. [15,16] agree with each other, their uncertainties are quite high (about 10 keV or higher) because within the framework of the transfer reactions, the excited levels are indirectly deduced from the energy and momentum distributions of the reaction products (charged particles), instead of the direct way, that is, from the γ transitions of the excited levels. The latter were also not reported in Refs. [15,16].

Apart from the above ion-induced experiments, the neutron-capture reactions also play an important role in the construction of the ^{153}Sm level scheme. In fact, by using the $(n_{\rm th}, \gamma)$ and $(n = 2$ keV$, \gamma)$ reactions ($n_{\rm th}$ means the thermal neutron with energy of 0.025 eV), Refs. [1,5,17,21] have thoughtfully investigated the level scheme of ^{153}Sm by means of the bent-crystal, conversion-electron, and Ge detector spectrometers. For the latter, the first two spectrometers, which were used to measure the low energy γ rays, focused on the low-energy part (below 0.4 MeV) of the ^{153}Sm level scheme, whereas the last one was used to detect the high-energy γ rays and to consequently deduce the feeding levels corresponding to the observed γ rays. Moreover, through the γ spectrum measured by the Ge detectors, 35 γ rays emitted from the compound state of ^{153}Sm via $(n_{\rm th}, \gamma)$ reaction were reported in Refs. [1,5,21]. Similarly, Ref. [17] has detected 31 γ rays via $(n = 2$ keV$, \gamma)$ reaction. Many excited levels, whose energies range from 0 to approximately 2.7 MeV, were also deduced from the γ rays detected in Ref. [17]. In general, the number of γ rays that can be detected by the conventional Ge detector spectrometer is restricted by the high Compton background of the γ spectrum as well as the energy resolution of the Ge detector. Besides, the γ spectrum of ^{153}Sm obtained from the (n, γ) reaction is always influenced by ^{150}Sm because the thermal neutron-capture cross section of ^{149}Sm is extremely higher than that of ^{152}Sm (see, e.g., Table I).

TABLE I. Isotopic content of the target used in the present experiment.

Isotope	Percentage (%)	$\sigma_{\rm th}$ (barn) [25]
^{152}Sm	98.7	206 ± 3
^{144}Sm	0.01	1.64 ± 0.10
^{147}Sm	0.06	57 ± 3
^{148}Sm	0.07	2.4 ± 0.6
^{149}Sm	0.13	40140 ± 600
^{150}Sm	0.20	100 ± 4
^{154}Sm	0.83	8.5 ± 0.5

Given the limitations of the works mentioned above, it is necessary to improve the level scheme of ^{153}Sm, especially in the energy region from 0.5 to about 5.0 MeV. One of the possibilities is to perform the ^{152}Sm$(n_{\rm th}, \gamma)$ reaction using an advance γ-γ coincidence technique together with the Ge(Li) detectors [also called the $(n, 2\gamma)$ technique or the method of digital summation amplitudes of coincident pulses] [22]. This technique, which has advantages in identifying the correlated γ transitions and in subtracting most of the Compton background, allows us to detect the two-step γ cascades (TSC) decayed from the compound state to the low-energy final levels and can therefore be used to deduce many new excited levels in ^{153}Sm within the energy region from 0.5 to 5.0 MeV and the spin range of $[\frac{1}{2}, \frac{3}{2}]\hbar$. Indeed, by using the above technique, we have successfully studied the updated level scheme of ^{172}Yb via ^{171}Yb$(n_{\rm th}, \gamma)$ reaction [23]. In particular, we have detected in the level scheme of ^{172}Yb several new excited levels and the corresponding γ transitions, whose data do not currently exist in the ENSDF library, especially those in the intermediate energy region from 3 to 5 MeV.

The goal of the present paper is to update the level scheme of ^{153}Sm via the $(n_{\rm th}, \gamma)$ reaction by using the γ-γ coincidence technique. The energy and spin regions to be covered by this experiment are [0.52, 5.3] MeV and $[\frac{1}{2}, \frac{3}{2}]\hbar$, respectively. In addition, by combining our newly updated levels with those presently existed in the ENSDF library, we are able to construct the new total and partial (within spin range of $[\frac{1}{2}, \frac{3}{2}]\hbar$) cumulative numbers of discrete levels, which are latter used to test the predictive power of various nuclear level density (NLD) models. At the same time, these new cumulative curves have also been compared with those extracted from the NLD data obtained using the Oslo method [24].

II. EXPERIMENTAL METHOD

The ^{152}Sm$(n_{\rm th}, \gamma)$ reaction was carried out at Dalat Nuclear Research Institute (Vietnam) using the thermal neutron beam from the tangential channel of Dalat Nuclear Research Reactor. The thermal neutron beam, which was obtained by using the filtered technique, has the size and flux at the irradiated position to be equal to 2.5 cm and 1.7×10^5 n cm^{-2} s^{-1}, respectively. This beam configuration is sufficient for the

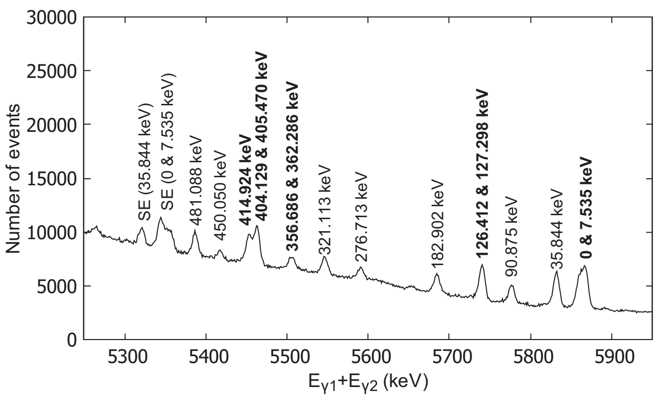

FIG. 1. Experimental summation spectrum of ^{153}Sm. The final energies E_f are marked on top of their corresponding peaks. The notation SE denotes the single-escape peaks.

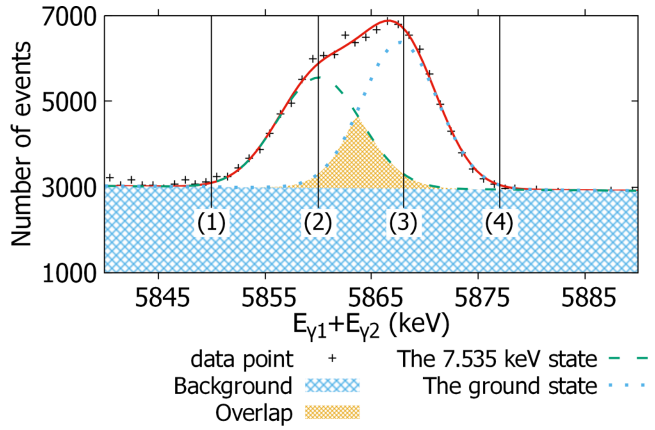

FIG. 2. Illustration of the gating windows used to reduce the contribution of the overlapped peaks. This figure shows the overlap of the summation peaks between the ground and 7.535-keV excited states.

present experiment as discussed, e.g., in Ref. [23]. The experimental setup and measurement using the γ-γ coincidence spectrometer with two HPGe detectors are the same as those presented in Ref. [23] (except the target nucleus), so we do not repeat them here.

The target nucleus ^{152}Sm is in the form of a 583 mg Sm_2O_3 powder. This target, which was put in a plastic bag, was then measured at the center of the thermal neutron beam for approximately 661 h. The isotopic content of the target, which is provided by the JSC Isotope Supplier, together with the thermal neutron-capture cross sections (σ_{th}) of all the isotopic components [25] are given in Table I.

Table I shows that ^{144,148,154}Sm isotopes have the values of both concentration and σ_{th} being significantly smaller than those of ^{152}Sm. Consequently, their influence on the spectroscopic data is negligible. For ^{147,150}Sm isotopes, although their σ_{th} values are comparable with that of ^{152}Sm, their impact on the spectroscopic data is still small because of their tiny percentages. The only samarium isotope which has a considerable influence on the spectroscopic data is ^{149}Sm because it has a noticeable σ_{th} value; namely, σ_{th} of ^{149}Sm is ≈198 times higher than that of ^{152}Sm. Therefore, despite the percentage of ^{149}Sm being ≈759 times less than that of ^{152}Sm, its contribution to the coincidence events caused by the thermal neutron capture of ^{149}Sm is only ≈3.8 times less than that of ^{152}Sm, implying that approximately 20% of all the detected coincidence events will be affected by the excited compound ^{150}Sm nucleus. Fortunately, the two-step cascades caused by ^{150}Sm can be distinguished from those of ^{153}Sm by using the γ-γ coincidence method because their summation energies (the total energy of two γ rays) are different. For instance, the summation energies of the cascades of ^{150}Sm detected within the present experiment range from ≈6.0 MeV to its neutron binding energy $B_n = 7.9867$ MeV [26], whereas those of ^{153}Sm vary from ≈5.2 to 5.87 MeV, as clearly seen in Fig. 1.

For every detected coincident event, the energies absorbed by two HPGe detectors are recorded. The γ cascades, which come from the decays of the compound state to the ground state and some defined final levels (via different intermediate levels), can be identified in the form of appropriate peaks appearing in the summation spectrum. The latter is obtained by counting the number of events per an interval of total energy absorbed by two HPGe detectors.

The most instructive part of the summation spectrum of ^{153}Sm is shown in Fig. 1. In this figure, all the γ cascades decayed from the compound state to the ground state and 15 final states, whose energies are 7.535, 35.844, 90.875, 126.412, 127.298, 182.902, 276.713, 321.113, 356.686, 362.286, 404.129, 405.470, 414.924, 450.050, and 481.088 keV,[1] can be identified based on their corresponding peaks. By gating on the appropriate peak, the TSC spectrum corresponding to the γ cascades from the compound state to a given final level is obtained. Figure 1 also shows some overlaps between different groups of states, whose energies are not much different, e.g., (0, 7.535 keV), (414.924, 404.129, and 405.470 keV), etc. The γ cascades coming from these overlapped peaks are indistinguishable because of the restricted energy resolution of the HPGe detectors used in the present experiment. However, these overlaps can be possibly reduced by a special selection of the gating window, as illustrated in Fig. 2. It can be seen in this Fig. 2 that an overlapped peak of two states can be fitted by two Gaussian functions, whose width and centroid position are different. Thus, the overlapped region can be easily identified if the gating window is divided into two regions. The first region is set between the lines (1) and (2) corresponding, respectively, to the head-tail and maximum positions of first Gaussian. The second region is chosen between the lines (3) and (4), which correspond to the maximum and end-tail positions of the second Gaussian, respectively. Once the overlapped region is identified (see the overlapped area in Fig. 2), its contribution can be easily reduced from the TSC spectrum. As a result, the contribution of the overlapped regions to the obtained TSC spectra is found to be less than 5%. However, it should be noted that the above

[1]It should be noted that the very precise energy values of the final levels given in the present paper are taken from Ref. [6].

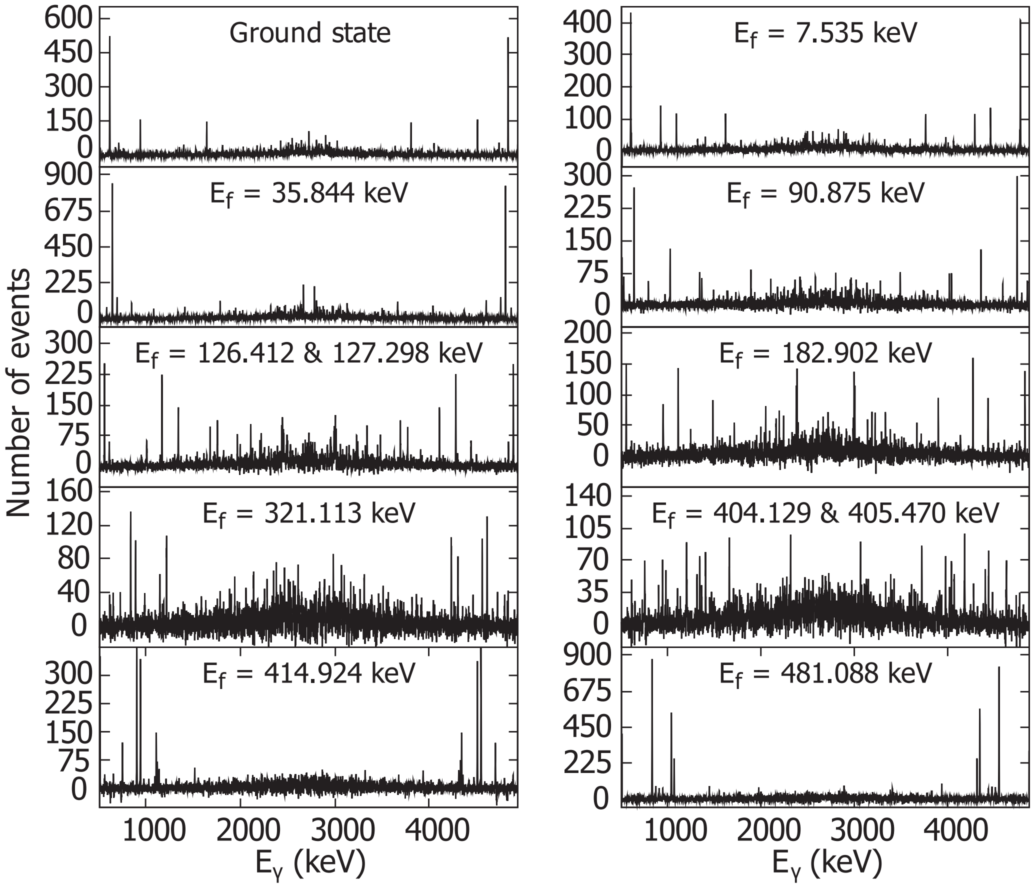

FIG. 3. Two-step cascade spectra of ^{153}Sm obtained for different final states E_f.

approach cannot be applied if energies of the overlapped peaks are notably close to each other, namely if the difference between energies of two peaks is smaller than 0.8 FWHM (full width at half maximum), e.g., the following pairs of final levels (126.412, 127.298) keV and (404.129, 405.470) keV.

All the measured TSC spectra are shown in Fig. 3. Because of low statistics, the TSC spectra corresponding to the following final levels 276.713, 356.686, 362.286, and 450.050 keV have not been analyzed yet. Although the energy resolutions of the two HPGe detectors used in the present experiment are slightly different, the obtained TSC spectra have mirror symmetry because an algorithm for improving the digital resolution [27] has been applied. The vicinity regions around each summation peak are gated to create a corresponding background spectrum. The latter is then subtracted from the spectrum obtained from the gating of the peak region, thus leading to some negative values in the TSC spectra in Fig. 3.

A pair of peaks, which are symmetric within a TSC spectrum, represent a γ cascade. The peak positions and areas correspond to the transition energies and intensities, respectively. In order to construct the nuclear level scheme, we assume that the γ transitions, which appear in more than one TSC spectrum, are considered to be the primary transitions. In addition, a transition is also considered as primary if it is currently determined as primary in the ENSDF library [7].

As for the spin of the levels, the possible spins of an observed intermediate level are often evaluated by using the following formula

$$\max(J_i - L, J_f - L) \leqslant J \leqslant \min(J_i + L, J_f + L), \quad (1)$$

where J_i, J, and J_f are spins of the initial, intermediate, and final levels, respectively, and L is the multipolarity. Within the present work, we assume that all the observed transitions are dipole ($L = 1$). This assumption is made because the probability of detecting the dipole transition is much higher than that of the quadrupole ($L = 2$) [28].

III. RESULTS AND DISCUSSION

A. Level scheme of ^{153}Sm

We have identified in total 576 γ transitions corresponding to 386 γ cascades, which are associated with the decays from the compound state to the ground state and 11 final levels (see Table II). The latter are 7.535 ($\frac{5}{2}^+$), 35.844 ($\frac{3}{2}^-$), 90.875 ($\frac{5}{2}^-$), 126.412 ($\frac{1}{2}^-$), 127.298 ($\frac{3}{2}^-$), 182.902 ($\frac{5}{2}^-$), 321.113 ($\frac{3}{2}^+$), 404.129 ($\frac{1}{2}^-$), 405.470 ($\frac{3}{2}^-$), 414.924 ($\frac{1}{2}^+$), and 481.088 ($\frac{3}{2}^+$) keV. Based on these observed cascades, we have determined 103 primary γ transitions corresponding to 103 intermediate levels and 299 secondary transitions emitted from these levels. Among the above primary transitions, 99 transitions have been deduced since they appear in more than one TSC spectrum. The remaining 4 transitions, whose energies are 4329.1, 4420.1, 4769.6, and 5133.2 keV, are also considered

TABLE II. γ-cascade transition energies and absolute intensities obtained from the ^{152}Sm(n_{th}, γ) reaction. Primary transitions and intermediate levels corresponding to each γ cascade are determined if possible. Comparisons between the data obtained within the present work with those extracted from the ENSDF library are made. Present work, experimental data obtained from the present work; ENSDF, data taken from the ENSDF library [6]; E_1, energy (in keV) of the primary γ transition; E_2, energy (in keV) of the secondary γ transition; E_i, energy (in keV) of the intermediate level; $I_{\gamma\gamma}$, absolute intensity of the cascade normalized to 10^6 decays (Uncertainties of the normalization factors are not taken into account); E_f, energy (in keV) of the final level (spin and parity of the final level are given in parentheses); J_i, tentative spin (in $\hbar$) of the corresponding level. Throughout the table, the uncertainty for numeric values is given next to the corresponding value (in *italic* type) and referred to the last digits of the value, e.g., 12.1 *23* means 12.1 ± 2.3. The experimental data within the present work, which agree with those existed in the ENSDF library, are highlighted in **bold** type.

Present Work						ENSDF		
E_1	E_i	J_i	E_2	$I_{\gamma\gamma}$	E_f	E_1[a]	E_i[b]	J_i
5238.0 *3*	**630.4 *7***	$\frac{3}{2}$	**630.4 *3***	5039 *327*	0 $(\frac{3}{2}^+)$	5237.8 *3*	630.20 *5*[f]	$\frac{1}{2}^-, \frac{3}{2}^-$
			622.9 *3*	3695 *316*	7.535 $(\frac{5}{2}^+)$			
			594.6 *4*	462 *98*	35.844 $(\frac{3}{2}^-)$			
			539.5 *3*	487 *95*	90.875 $(\frac{5}{2}^-)$			
[x]5231.2 *4*			[x]629.7 *4*	485 *114*	7.535 $(\frac{5}{2}^+)$			
5172.7 *4*	**695.7 *8***	$\frac{3}{2}$	696.0 *4*	312 *77*	0 $(\frac{3}{2}^+)$	5172.7 *3*	695.80 *4*[g]	$\frac{1}{2}^-$
			659.6 *3*	4562 *321*	35.844 $(\frac{3}{2}^-)$			
			604.8 *5*	175 *54*	90.875 $(\frac{5}{2}^-)$			
			568.2 *3*	1121 *139*	126.412 $(\frac{1}{2}^-)$[c]			
5133.2 *3*	**735.2 *7***	$\frac{1}{2}, \frac{3}{2}$	**735.2 *3***	553 *104*	0 $(\frac{3}{2}^+)$	5133.3 *8*	734.873 *23*[h]	$(\frac{3}{2}^+, \frac{5}{2})$
5118.3 *4*	**750.1 *8***	$\frac{3}{2}$	**750.4 *5***	267 *70*	0 $(\frac{3}{2}^+)$	5117.8 *5*	750.32 *5*	$(\frac{3}{2})^-$
			714.1 *3*	805 *133*	35.844 $(\frac{3}{2}^-)$			
			659.3 *3*	1808 *192*	90.875 $(\frac{5}{2}^-)$			
			622.6 *4*	306 *71*	126.412 $(\frac{1}{2}^-)$[c]			
			567.2 *3*	693 *130*	182.902 $(\frac{5}{2}^-)$			
[x]5100.2 *6*			[x]768.2 *6*	124 *51*	0 $(\frac{3}{2}^+)$			
5079.9 *5*	**788.5 *9***	$\frac{3}{2}$	788.9 *5*	250 *68*	0 $(\frac{3}{2}^+)$	5078.86	788.92 *5*	$\frac{3}{2}^+$
			780.5 *6*	186 *63*	7.535 $(\frac{5}{2}^+)$			
4951.5 *3*	**916.9 *7***	$\frac{3}{2}$	881.1 *3*	654 *119*	35.844 $(\frac{3}{2}^-)$	4951.5 *6*	917.1 *5*	$(\frac{3}{2}^+)$
			826.0 *3*	324 *77*	90.875 $(\frac{5}{2}^-)$			
4884.6 *5*	**983.8 *9***	$\frac{3}{2}$	984.3 *3*	1576 *130*	0 $(\frac{3}{2}^+)$	4884.0 *8*	984.2 *4*[i]	$\frac{3}{2}^+$
			976.8 *3*	1302 *151*	7.535 $(\frac{5}{2}^+)$			
			947.2 *6*	154 *49*	35.844 $(\frac{3}{2}^-)$			
			801.6 *5*	143 *47*	182.902 $(\frac{5}{2}^-)$			
			662.0 *5*	169 *60*	321.113 $(\frac{3}{2}^+)$			
			568.6 *7*	234 *96*	414.924 $(\frac{1}{2}^+)$			
[x]4810.1 *5*			[x]737.2 *5*	109 *43*	321.113 $(\frac{3}{2}^+)$			
[x]4806.1 *8*			[x]581.2 *8*	194 *92*	481.088 $(\frac{3}{2}^+)$			
[x]4794.2 *6*			[x]659.3 *6*	159 *76*	414.924 $(\frac{1}{2}^+)$			
4769.6 *4*	**1098.8 *8***	$\frac{1}{2}, \frac{3}{2}$	1098.8 *4*	216 *50*	0 $(\frac{3}{2}^+)$	4770.57	1097.8 *5*	$\frac{1}{2}^+, \frac{3}{2}^+$
4757.4 *6*	**1111.0 *10***	$\frac{3}{2}$	1074.5 *5*	202 *57*	35.844 $(\frac{3}{2}^-)$	4757.9 *7*	1109.7 *4*	$\frac{1}{2}^+, \frac{3}{2}^+$
			1020.6 *6*	98 *39*	90.875 $(\frac{5}{2}^-)$			
			984.5 *5*	97 *37*	126.412 $(\frac{1}{2}^-)$[c]			
			927.3 *6*	97 *36*	182.902 $(\frac{5}{2}^-)$			
[x]4724.2 *4*			[x]738.7 *4*	128 *40*	404.129 $(\frac{1}{2}^-)$[d]			
[x]4719.4 *7*			[x]827.9 *7*	45 *23*	321.113 $(\frac{3}{2}^+)$			
[x]4711.0 *8*			[x]1030.1 *8*	70 *30*	126.412 $(\frac{1}{2}^-)$[c]			

(Continued.)

Present Work					ENSDF			
E_1	E_i	J_i	E_2	$I_{\gamma\gamma}$	E_f	E_1[a]	E_i[b]	J_i
4704.8 6	1163.6 10	$\frac{1}{2}, \frac{3}{2}$	1163.5 5	144 45	0 $(\frac{3}{2}^+)$			
			1036.4 7	66 30	126.412 $(\frac{1}{2}^-)$[c]			
4697.4 4	**1171.0 8**	$\frac{3}{2}$	1171.3 4	190 58	0 $(\frac{3}{2}^+)$	4697.2 7	1171.1 3	$\frac{1}{2}^-, \frac{3}{2}^-$
			1163.0 3	1132 167	7.535 $(\frac{5}{2}^+)$			
			1134.5 4	377 81	35.844 $(\frac{3}{2}^-)$			
			1079.9 3	843 111	90.875 $(\frac{5}{2}^-)$			
			1044.2 4	345 72	126.412 $(\frac{1}{2}^-)$[c]			
			988.3 3	537 89	182.902 $(\frac{5}{2}^-)$			
			849.4 3	701 112	321.113 $(\frac{3}{2}^+)$			
			766.1 4	430 88	404.129 $(\frac{1}{2}^-)$[d]			
			755.4 4	701 172	414.924 $(\frac{1}{2}^+)$			
			691.0 8	188 89	481.088 $(\frac{3}{2}^+)$			
[x]4676.6 9			[x]870.7 9	51 24	321.113 $(\frac{3}{2}^+)$			
[x]4674.2 6			[x]713.1 6	117 56	481.088 $(\frac{3}{2}^+)$			
4645.1 4	**1223.3 8**	$\frac{1}{2}, \frac{3}{2}$	1223.2 5	191 54	0 $(\frac{3}{2}^+)$	4644.6 10	1224.3 4	$(\frac{3}{2})^+$
			902.0 3	505 94	321.113 $(\frac{3}{2}^+)$			
4546.2 5	**1322.2 9**	$\frac{1}{2}, \frac{3}{2}$	1195.3 6	64 28	126.412 $(\frac{1}{2}^-)$[c]	4545.7 4	1322.1 3	$\frac{1}{2}^-, \frac{3}{2}^-$
			1000.7 5	167 52	321.113 $(\frac{3}{2}^+)$			
			917.2 6	170 57	404.129 $(\frac{1}{2}^-)$[d]			
			906.9 3	2174 315	414.924 $(\frac{1}{2}^+)$			
			840.8 3	4053 379	481.088 $(\frac{3}{2}^+)$			
4525.4 4	**1343.0 8**	$\frac{3}{2}$	1215.9 3	1058 121	126.412 $(\frac{1}{2}^-)$[c]	4525.29	1344.0 6	$(\frac{3}{2})^+$
			1160.2 3	761 110	182.902 $(\frac{5}{2}^-)$			
			937.3 4	75 22	404.129 $(\frac{1}{2}^-)$[d]			
[x]4518.0 5			[x]945.0 5	63 24	404.129 $(\frac{1}{2}^-)$[d]			
4507.4 4	**1361.0 8**	$\frac{1}{2}, \frac{3}{2}$	945.9 3	1712 220	414.924 $(\frac{1}{2}^+)$	4507.41	1360.9 5	$\frac{1}{2}^-, \frac{3}{2}^-$
			880.3 5	384 111	481.088 $(\frac{3}{2}^+)$			
4503.2 4	1365.2 8	$\frac{3}{2}$	1274.1 6	180 52	90.875 $(\frac{5}{2}^-)$			
			960.1 3	368 64	404.129 $(\frac{1}{2}^-)$[d]			
4475.7 7	**1392.7 11**	$\frac{1}{2}, \frac{3}{2}$	987.5 5	90 29	404.129 $(\frac{1}{2}^-)$[d]	4474.4 8	1393.9 8[f]	
			977.4 9	87 49	414.924 $(\frac{1}{2}^+)$			
4471.4 6	**1397.0 10**	$\frac{1}{2}, \frac{3}{2}$	982.3 8	118 57	414.924 $(\frac{1}{2}^+)$	4472.76	1395.6 6	$\frac{3}{2}^+, \frac{5}{2}^+$
			915.7 5	371 107	481.088 $(\frac{3}{2}^+)$			
4467.6 4	**1400.8 8**	$\frac{1}{2}, \frac{3}{2}$	1400.5 4	220 62	0 $(\frac{3}{2}^+)$	4468.3 8	1400.0 8	$(\frac{5}{2}^-)$
			995.7 3	296 58	404.129 $(\frac{1}{2}^-)$[d]			
[x]4456.3 5			[x]1412.1 5	141 49	0 $(\frac{3}{2}^+)$			
4445.6 4	**1422.8 8**	$\frac{3}{2}$	1414.6 4	314 76	7.535 $(\frac{5}{2}^+)$	4446.81	1421.5 7	$\frac{1}{2}^+, \frac{3}{2}^+$
			1018.1 4	132 37	404.129 $(\frac{1}{2}^-)$[d]			
4432.6 5	**1435.8 9**	$\frac{1}{2}, \frac{3}{2}$	1436.1 4	385 82	0 $(\frac{3}{2}^+)$	4432.97	1435.4 3	$\frac{1}{2}^+, \frac{3}{2}^+$
			1114.5 7	90 40	321.113 $(\frac{3}{2}^+)$			
			954.8 4	366 104	481.088 $(\frac{3}{2}^+)$			
[x]4424.4 6			[x]1038.6 6	69 29	404.129 $(\frac{1}{2}^-)$[d]			
[x]4422.7 9			[x]964.6 9	152 65	481.088 $(\frac{3}{2}^+)$			
4420.1 7	**1448.3 11**	$\frac{1}{2}, \frac{3}{2}$	1033.4 7	160 61	414.924 $(\frac{1}{2}^+)$	4420.73	1447.6 4	$(\frac{3}{2})^-$

(Continued.)

Present Work					ENSDF			
E_1	E_i	J_i	E_2	$I_{\gamma\gamma}$	E_f	E_1[a]	E_i[b]	J_i
[x]4417.8 *4*			[x]1414.8 *4*	284 *67*	35.844 $(\frac{3}{2}^-)$			
[x]4401.0 *7*			[x]1340.1 *7*	85 *32*	126.412 $(\frac{1}{2}^-)$[c]			
4382.1 *5*	**1486.3 *9***	$\boldsymbol{\frac{3}{2}}$	1486.8 *4*	398 *93*	0 $(\frac{3}{2}^+)$	4382.60	1485.7 *4*	$(\frac{3}{2}^+)$
			1450.7 *6*	144 *46*	35.844 $(\frac{3}{2}^-)$			
			1359.3 *6*	77 *33*	126.412 $(\frac{1}{2}^-)$[c]			
			1303.0 *6*	168 *51*	182.902 $(\frac{5}{2}^-)$			
			1164.4 *4*	344 *83*	321.113 $(\frac{3}{2}^+)$			
			1071.5 *8*	78 *39*	414.924 $(\frac{1}{2}^+)$			
[x]4376.9 *8*			[x]1170.4 *8*	66 *32*	321.113 $(\frac{3}{2}^+)$			
4354.7 *5*	**1513.7 *9***	$\boldsymbol{\frac{3}{2}}$	1506.2 *4*	355 *81*	7.535 $(\frac{5}{2}^+)$	4355.51	1512.8 *3*	$(\frac{3}{2}^+)$
			1477.7 *5*	186 *53*	35.844 $(\frac{3}{2}^-)$			
			1423.0 *3*	534 *96*	90.875 $(\frac{5}{2}^-)$			
			1193.1 *6*	114 *43*	321.113 $(\frac{3}{2}^+)$			
			1098.3 *5*	201 *68*	414.924 $(\frac{1}{2}^+)$			
4340.9 *4*	**1527.5 *8***	$\boldsymbol{\frac{1}{2}, \frac{3}{2}}$	1491.6 *3*	491 *88*	35.844 $(\frac{3}{2}^-)$	4341.4 *15*	1527.0 *5*	$(\frac{1}{2}^-, \frac{3}{2}^-)$
			1400.2 *3*	688 *93*	126.412 $(\frac{1}{2}^-)$[c]			
			1206.1 *5*	149 *50*	321.113 $(\frac{3}{2}^+)$			
			1122.3 *4*	215 *58*	404.129 $(\frac{1}{2}^-)$[d]			
			1046.3 *3*	2820 *296*	481.088 $(\frac{3}{2}^+)$			
4329.1 *3*	**1539.3 *7***	$\boldsymbol{\frac{3}{2}}$	1448.4 *3*	348 *79*	90.875 $(\frac{5}{2}^-)$	4330.24	1538.1 *5*	$\frac{1}{2}^+, \frac{3}{2}^+$
4311.0 *4*	**1557.4 *8***	$\boldsymbol{\frac{1}{2}, \frac{3}{2}}$	1521.6 *4*	234 *59*	35.844 $(\frac{3}{2}^-)$	4310.6 *15*	1557.7 *15*	$\frac{1}{2}^+, \frac{3}{2}^+$
			1430.5 *5*	112 *37*	126.412 $(\frac{1}{2}^-)$[c]			
			1236.2 *3*	540 *103*	321.113 $(\frac{3}{2}^+)$			
			1076.2 *3*	1267 *196*	481.088 $(\frac{3}{2}^+)$			
4242.1 *4*	1626.3 *8*	$\frac{1}{2}, \frac{3}{2}$	1626.7 *5*	326 *73*	0 $(\frac{3}{2}^+)$			
			1220.4 *3*	551 *93*	404.129 $(\frac{1}{2}^-)$[d]			
[x]4240.1 *6*			[x]1307.2 *6*	98 *39*	321.113 $(\frac{3}{2}^+)$			
[x]4233.8 *8*			[x]1229.1 *8*	92 *38*	404.129 $(\frac{1}{2}^-)$[d]			
4207.8 *6*	**1660.6 *10***	$\boldsymbol{\frac{3}{2}}$	1624.9 *6*	163 *51*	35.844 $(\frac{3}{2}^-)$		1662	$(\frac{3}{2})^+$
			1477.6 *6*	83 *34*	182.902 $(\frac{5}{2}^-)$			
[x]4191.8 *4*			[x]1585.8 *4*	184 *51*	90.875 $(\frac{5}{2}^-)$			
[x]4143.3 *6*			[x]1597.8 *6*	76 *31*	126.412 $(\frac{1}{2}^-)$[c]			
4128.7 *5*	1739.7 *9*	$\frac{3}{2}$	1740.3 *3*	324 *75*	0 $(\frac{3}{2}^+)$			
			1648.5 *6*	131 *45*	90.875 $(\frac{5}{2}^-)$			
			1612.2 *5*	162 *47*	126.412 $(\frac{1}{2}^-)$[c]			
			1556.5 *3*	411 *81*	182.902 $(\frac{5}{2}^-)$			
			1418.0 *8*	116 *50*	321.113 $(\frac{3}{2}^+)$			
			1333.8 *3*	280 *62*	404.129 $(\frac{1}{2}^-)$[d]			
			1258.9 *8*	87 *45*	481.088 $(\frac{3}{2}^+)$			
4115.9 *5*	**1752.5 *9***	$\boldsymbol{\frac{3}{2}}$	1752.7 *3*	1377 *157*	0 $(\frac{3}{2}^+)$		1751.4 *5*	$\frac{1}{2}, \frac{3}{2}$
			1745.3 *3*	1044 *146*	7.535 $(\frac{5}{2}^+)$			
			1624.1 *6*	92 *33*	126.412 $(\frac{1}{2}^-)$[c]			
			1431.9 *8*	138 *55*	321.113 $(\frac{3}{2}^+)$			

(Continued.)

Present Work					ENSDF			
E_1	E_i	J_i	E_2	$I_{\gamma\gamma}$	E_f	E_1[a]	E_i[b]	J_i
[x]4114.1 *5*			[x]1273.2 *5*	136 *53*	481.088 $(\frac{3}{2}^+)$			
4099.8 *5*	1768.6 *9*	$\frac{1}{2},\frac{3}{2}$	1768.2 *5*	238 *71*	0 $(\frac{3}{2}^+)$			
			1732.7 *5*	181 *57*	35.844 $(\frac{3}{2}^-)$			
			1363.7 *3*	408 *75*	404.129 $(\frac{1}{2}^-)$[d]			
[x]4095.3 *8*			[x]1773.1 *8*	136 *56*	0 $(\frac{3}{2}^+)$			
4078.4 *5*	1790.0 *9*	$\frac{3}{2}$	1789.7 *4*	257 *67*	0 $(\frac{3}{2}^+)$			
			1607.0 *6*	104 *39*	182.902 $(\frac{5}{2}^-)$			
			1384.8 *4*	236 *56*	404.129 $(\frac{1}{2}^-)$[d]			
[x]4074.8 *8*			[x]1472.5 *8*	84 *40*	321.113 $(\frac{3}{2}^+)$			
4035.1 *5*	**1833.3** ***9***	$\frac{3}{2}$	1797.0 *5*	172 *56*	35.844 $(\frac{3}{2}^-)$		1833	$(\frac{5}{2})^+$
			1743.2 *6*	153 *53*	90.875 $(\frac{5}{2}^-)$			
			1427.4 *3*	418 *75*	404.129 $(\frac{1}{2}^-)$[d]			
4027.0 *5*	**1841.4** ***9***	$\frac{3}{2}$	1805.5 *4*	259 *68*	35.844 $(\frac{3}{2}^-)$		1840	$(\frac{5}{2})^+$
			1750.6 *5*	212 *58*	90.875 $(\frac{5}{2}^-)$			
[x]4024.3 *7*			[x]1661.2 *7*	141 *47*	182.902 $(\frac{5}{2}^-)$			
[x]4019.5 *5*			[x]1721.6 *5*	103 *36*	126.412 $(\frac{1}{2}^-)$[c]			
3992.2 *5*	1876.2 *9*	$\frac{3}{2}$	1785.1 *6*	152 *48*	90.875 $(\frac{5}{2}^-)$			
			1471.0 *5*	112 *37*	404.129 $(\frac{1}{2}^-)$[d]			
3983.0 *5*	**1885.4** ***9***	$\frac{1}{2},\frac{3}{2}$	1758.1 *3*	336 *61*	126.412 $(\frac{1}{2}^-)$[c]		1884	$(\frac{5}{2}^-,\frac{7}{2}^-)$
			1480.0 *6*	143 *43*	404.129 $(\frac{1}{2}^-)$[d]			
[x]3981.2 *6*			[x]1796.3 *6*	133 *45*	90.875 $(\frac{5}{2}^-)$			
[x]3970.8 *4*			[x]1492.2 *4*	186 *50*	404.129 $(\frac{1}{2}^-)$[d]			
[x]3956.3 *4*			[x]1506.7 *4*	146 *42*	404.129 $(\frac{1}{2}^-)$[d]			
[x]3945.4 *6*			[x]1601.8 *6*	100 *40*	321.113 $(\frac{3}{2}^+)$			
3942.6 ***5***	**1925.8** ***9***	$\frac{1}{2},\boldsymbol{\frac{3}{2}}$	1798.3 *6*	129 *38*	126.412 $(\frac{1}{2}^-)$[c]	3943.5 *8*	1924.9 *8*	$\frac{3}{2}^+,\frac{5}{2}^+$
			1520.7 *5*	139 *44*	404.129 $(\frac{1}{2}^-)$[d]			
3934.9 ***5***	**1933.5** ***9***	$\frac{1}{2},\frac{3}{2}$	1897.6 *3*	705 *111*	35.844 $(\frac{3}{2}^-)$	3934.6 *6*	1933.8	$(\frac{5}{2})^+$
			1806.8 *4*	164 *42*	126.412 $(\frac{1}{2}^-)$[c]			
			1613.4 *6*	200 *63*	321.113 $(\frac{3}{2}^+)$			
			1451.5 *4*	300 *90*	481.088 $(\frac{3}{2}^+)$			
3932.3 *5*	1936.1 *9*	$\frac{3}{2}$	1936.5 *4*	415 *91*	0 $(\frac{3}{2}^+)$			
			1929.4 *5*	317 *80*	7.535 $(\frac{5}{2}^+)$			
			1844.9 *5*	183 *55*	90.875 $(\frac{5}{2}^-)$			
			1752.2 *5*	105 *41*	182.902 $(\frac{5}{2}^-)$			
[x]3900.7 *3*			[x]1840.4 *3*	530 *76*	126.412 $(\frac{1}{2}^-)$[c]			
[x]3887.8 *6*			[x]1659.5 *6*	145 *51*	321.113 $(\frac{3}{2}^+)$			
[x]3885.2 *4*			[x]1800.3 *4*	219 *62*	182.902 $(\frac{5}{2}^-)$			
3830.9 *5*	2037.5 *9*	$\frac{1}{2},\frac{3}{2}$	2037.3 *5*	218 *65*	0 $(\frac{3}{2}^+)$			
			2001.7 *4*	305 *72*	35.844 $(\frac{3}{2}^-)$			
			1910.3 *6*	183 *54*	126.412 $(\frac{1}{2}^-)$[c]			
			1556.7 *5*	229 *81*	481.088 $(\frac{3}{2}^+)$			
[x]3829.3 *6*			[x]1948.3 *6*	155 *54*	90.875 $(\frac{5}{2}^-)$			
[x]3781.5 *6*			[x]2086.9 *6*	226 *77*	0 $(\frac{3}{2}^+)$			
3777.4 *5*	**2091.0** ***9***	$\frac{1}{2},\boldsymbol{\frac{3}{2}}$	2055.2 *5*	226 *62*	35.844 $(\frac{3}{2}^-)$		2092	$(\frac{3}{2})^+$

(Continued.)

Present Work					ENSDF			
E_1	E_i	J_i	E_2	$I_{\gamma\gamma}$	E_f	E_1[a]	E_i[b]	J_i
			1685.5 *3*	483 *91*	404.129 ($\frac{1}{2}^-$)[d]			
			1610.0 *7*	222 *82*	481.088 ($\frac{3}{2}^+$)			
3757.3 *4*	2111.1 *8*	$\frac{3}{2}$	2075.2 *4*	406 *86*	35.844 ($\frac{3}{2}^-$)			
			2020.4 *3*	572 *108*	90.875 ($\frac{5}{2}^-$)			
[x]3754.5 *7*			[x]1931.0 *7*	101 *45*	182.902 ($\frac{5}{2}^-$)			
[x]3752.1 *10*			[x]2080.5 *10*	127 *51*	35.844 ($\frac{3}{2}^-$)			
[x]3736.4 *8*			[x]1949.0 *8*	94 *42*	182.902 ($\frac{5}{2}^-$)			
3733.0 *6*	**2135.4 *10***	$\frac{1}{2}$, $\mathbf{\frac{3}{2}}$	1814.0 *6*	189 *64*	321.113 ($\frac{3}{2}^+$)		2135	$\frac{3}{2}^+$, $\frac{5}{2}^+$
			1730.3 *6*	138 *54*	404.129 ($\frac{1}{2}^-$)[d]			
3709.8 *6*	2158.6 *10*	$\frac{3}{2}$	2122.6 *5*	299 *77*	35.844 ($\frac{3}{2}^-$)		[e]2167 *13*	
			1974.9 *7*	122 *54*	182.902 ($\frac{5}{2}^-$)			
			1754.1 *6*	174 *56*	404.129 ($\frac{1}{2}^-$)[d]			
3693.6 *6*	2174.8 *10*	$\frac{1}{2}$, $\frac{3}{2}$	2174.5 *5*	369 *97*	0 ($\frac{3}{2}^+$)		[e]2167 *13*	
			2139.4 *7*	169 *59*	35.844 ($\frac{3}{2}^-$)			
			1769.3 *5*	156 *54*	404.129 ($\frac{1}{2}^-$)[d]			
3676.1 *5*	2192.3 *9*	$\frac{1}{2}$, $\frac{3}{2}$	2156.2 *4*	276 *74*	35.844 ($\frac{3}{2}^-$)		[e]2188 *15*	
			2065.1 *4*	261 *62*	126.412 ($\frac{1}{2}^-$)[c]			
			1711.5 *7*	157 *75*	481.088 ($\frac{3}{2}^+$)			
[x]3655.6 *6*			[x]1807.3 *6*	164 *56*	404.129 ($\frac{1}{2}^-$)[d]			
3644.6 *6*	2223.8 *10*	$\frac{1}{2}$, $\frac{3}{2}$	2097.0 *5*	223 *80*	126.412 ($\frac{1}{2}^-$)[c]			
			1817.8 *7*	161 *55*	404.129 ($\frac{1}{2}^-$)[d]			
3630.7 *7*	**2237.7 *11***	$\frac{3}{2}$	2229.3 *4*	186 *58*	7.535 ($\frac{5}{2}^+$)		2239 *12*	
			2054.9 *7*	152 *56*	182.902 ($\frac{5}{2}^-$)			
			1917.3 *7*	127 *53*	321.113 ($\frac{3}{2}^+$)			
[x]3611.2 *7*			[x]1936.1 *7*	91 *43*	321.113 ($\frac{3}{2}^+$)			
[x]3607.8 *6*			[x]1779.5 *6*	177 *77*	481.088 ($\frac{3}{2}^+$)			
[x]3582.2 *5*			[x]2103.3 *5*	236 *69*	182.902 ($\frac{5}{2}^-$)			
3574.8 *6*	2293.6 *10*	$\frac{1}{2}$, $\frac{3}{2}$	1972.0 *6*	177 *68*	321.113 ($\frac{3}{2}^+$)		[e]2286 *11*	
			1888.7 *6*	160 *56*	404.129 ($\frac{1}{2}^-$)[d]			
[x]3569.2 *8*			[x]2171.9 *8*	164 *63*	126.412 ($\frac{1}{2}^-$)[c]			
[x]3544.3 *5*			[x]2288.3 *5*	212 *62*	35.844 ($\frac{3}{2}^-$)			
[x]3539.9 *7*			[x]2145.6 *7*	154 *59*	182.902 ($\frac{5}{2}^-$)			
3533.5 *6*	2334.9 *10*	$\frac{3}{2}$	2334.8 *4*	440 *112*	0 ($\frac{3}{2}^+$)		[e]2332 *15*	
			2152.1 *7*	119 *49*	182.902 ($\frac{5}{2}^-$)			
3526.2 *5*	2342.2 *9*	$\frac{3}{2}$	2305.5 *5*	225 *66*	35.844 ($\frac{3}{2}^-$)		[e]2332 *15*	
			2250.8 *4*	262 *83*	90.875 ($\frac{5}{2}^-$)			
			2215.7 *4*	510 *114*	126.412 ($\frac{1}{2}^-$)[c]			
			2159.6 *4*	417 *96*	182.902 ($\frac{5}{2}^-$)			
			2021.3 *7*	178 *61*	321.113 ($\frac{3}{2}^+$)			
[x]3506.4 *7*			[x]2234.7 *7*	235 *78*	126.412 ($\frac{1}{2}^-$)[c]			
[x]3482.0 *6*			[x]2203.5 *6*	231 *70*	182.902 ($\frac{5}{2}^-$)			
[x]3479.9 *6*			[x]2067.4 *6*	128 *50*	321.113 ($\frac{3}{2}^+$)			
[x]3475.5 *5*			[x]1987.5 *5*	251 *70*	404.129 ($\frac{1}{2}^-$)[d]			
3453.1 *6*	2415.3 *10*	$\frac{1}{2}$, $\frac{3}{2}$	2094.2 *6*	153 *57*	321.113 ($\frac{3}{2}^+$)		[e]2413 *15*	

(Continued.)

Present Work					ENSDF			
E_1	E_i	J_i	E_2	$I_{\gamma\gamma}$	E_f	E_1[a]	E_i[b]	J_i
			2009.7 *6*	209 *64*	404.129 $(\frac{1}{2}^-)$[d]			
3448.9 *5*	2419.5 *9*	$\frac{3}{2}$	2412.5 *5*	339 *84*	7.535 $(\frac{5}{2}^+)$		[e]2413 *15*	
			2328.0 *5*	196 *75*	90.875 $(\frac{5}{2}^-)$			
3440.5 *7*	2427.9 *11*	$\frac{3}{2}$	2336.4 *9*	114 *51*	90.875 $(\frac{5}{2}^-)$		[e]2413 *15*	
			2023.0 *6*	233 *68*	404.129 $(\frac{1}{2}^-)$[d]			
3420.8 *6*	2447.6 *10*	$\frac{1}{2}, \frac{3}{2}$	2319.9 *4*	267 *60*	126.412 $(\frac{1}{2}^-)$[c]		[e]2456 *11*	
			1967.0 *8*	186 *81*	481.088 $(\frac{3}{2}^+)$			
3407.3 *4*	2461.1 *8*	$\frac{3}{2}$	2278.1 *4*	357 *89*	182.902 $(\frac{5}{2}^-)$		[e]2456 *11*	
			1980.1 *5*	294 *100*	481.088 $(\frac{3}{2}^+)$			
[x]3396.8 *5*			[x]2344.3 *5*	131 *43*	126.412 $(\frac{1}{2}^-)$[c]			
[x]3388.9 *7*			[x]2158.4 *7*	92 *46*	321.113 $(\frac{3}{2}^+)$			
3384.7 *7*	**2483.7** ***11***	$\frac{1}{2}, \frac{3}{2}$	2356.4 *6*	121 *40*	126.412 $(\frac{1}{2}^-)$[c]		2484 *11*	
			2078.3 *6*	191 *63*	404.129 $(\frac{1}{2}^-)$[d]			
			2002.6 *8*	240 *96*	481.088 $(\frac{3}{2}^+)$			
3373.7 *6*	**2494.7** ***10***	$\boldsymbol{\frac{3}{2}}$	2487.9 *5*	339 *83*	7.535 $(\frac{5}{2}^+)$		2496.6 *12*[j]	$\frac{1}{2}, \frac{3}{2}, \frac{5}{2}$
			2458.7 *6*	263 *73*	35.844 $(\frac{3}{2}^-)$			
3371.3 ***5***	**2497.1** ***9***	$\boldsymbol{\frac{3}{2}}$	2497.8 *5*	404 *102*	0 $(\frac{3}{2}^+)$	3371.8 *12*	2496.6 *12*[j]	$\frac{1}{2}, \frac{3}{2}, \frac{5}{2}$
			2405.8 *7*	288 *85*	90.875 $(\frac{5}{2}^-)$			
			2369.7 *5*	234 *56*	126.412 $(\frac{1}{2}^-)$[c]			
			2313.8 *5*	311 *83*	182.902 $(\frac{5}{2}^-)$			
			2176.4 *5*	370 *96*	321.113 $(\frac{3}{2}^+)$			
[x]3366.4 *7*			[x]2411.2 *7*	160 *63*	90.875 $(\frac{5}{2}^-)$			
3355.2 *5*	2513.2 *9*	$\frac{3}{2}$	2477.7 *3*	520 *87*	35.844 $(\frac{3}{2}^-)$		[e]2506 *14*	
			2329.9 *6*	152 *53*	182.902 $(\frac{5}{2}^-)$			
[x]3338.2 *6*			[x]2402.9 *6*	117 *39*	126.412 $(\frac{1}{2}^-)$[c]			
3325.8 *5*	2542.6 *9*	$\frac{3}{2}$	2535.0 *7*	142 *54*	7.535 $(\frac{5}{2}^+)$		[e]2534 *11*	
			2506.6 *5*	196 *54*	35.844 $(\frac{3}{2}^-)$			
			2451.2 *6*	277 *87*	90.875 $(\frac{5}{2}^-)$			
			2222.2 *4*	164 *61*	321.113 $(\frac{3}{2}^+)$			
3322.9 *6*	2545.5 *10*	$\frac{3}{2}$	2418.0 *5*	237 *56*	126.412 $(\frac{1}{2}^-)$[c]			
			2363.7 *5*	298 *77*	182.902 $(\frac{5}{2}^-)$			
[x]3318.5 *5*			[x]2542.4 *5*	238 *66*	7.535 $(\frac{5}{2}^+)$			
[x]3272.3 *7*			[x]2275.0 *7*	127 *45*	321.113 $(\frac{3}{2}^+)$			
[x]3264.1 *7*			[x]2283.2 *7*	77 *37*	321.113 $(\frac{3}{2}^+)$			
[x]3261.0 *4*			[x]2607.4 *4*	607 *119*	0 $(\frac{3}{2}^+)$			
[x]3259.1 *6*			[x]2573.5 *6*	189 *55*	35.844 $(\frac{3}{2}^-)$			
[x]3252.5 *4*			[x]2294.8 *4*	120 *39*	321.113 $(\frac{3}{2}^+)$			
[x]3250.6 *7*			[x]2212.4 *7*	167 *59*	404.129 $(\frac{1}{2}^-)$[d]			
[x]3230.8 *4*			[x]2601.8 *4*	286 *65*	35.844 $(\frac{3}{2}^-)$			
3224.9 ***5***	**2643.5** ***9***	$\boldsymbol{\frac{1}{2}, \frac{3}{2}}$	2643.6 *5*	302 *84*	0 $(\frac{3}{2}^+)$	3225.6 *7*	2642.8 *7*	$\frac{1}{2}, \frac{3}{2}, \frac{5}{2}$
			2322.3 *4*	227 *63*	321.113 $(\frac{3}{2}^+)$			
[x]3223.2 *8*			[x]2239.7 *8*	119 *56*	404.129 $(\frac{1}{2}^-)$[d]			
3196.2 *5*	2672.2 *9*	$\frac{3}{2}$	2672.3 *6*	285 *94*	0 $(\frac{3}{2}^+)$		[e]2669 *15*	
			2664.2 *5*	242 *70*	7.535 $(\frac{5}{2}^+)$			

(Continued.)

Present Work					ENSDF			
E_1	E_i	J_i	E_2	$I_{\gamma\gamma}$	E_f	E_1[a]	E_i[b]	J_i
			2636.4 *3*	482 *84*	35.844 $(\frac{3}{2}^-)$			
			2545.2 *6*	177 *54*	126.412 $(\frac{1}{2}^-)$[c]			
			2266.8 *5*	271 *79*	404.129 $(\frac{1}{2}^-)$[d]			
3190.6 *7*	2677.8 *11*	$\frac{1}{2}, \frac{3}{2}$	2677.7 *6*	391 *107*	0 $(\frac{3}{2}^+)$		[e]2669 *15*	
			2272.4 *9*	121 *59*	404.129 $(\frac{1}{2}^-)$[d]			
3187.3 *3*	2681.1 *7*	$\frac{3}{2}$	2645.5 *3*	508 *87*	35.844 $(\frac{3}{2}^-)$		[e]2686 *11*	
			2589.9 *4*	455 *108*	90.875 $(\frac{5}{2}^-)$			
3176.8 *5*	2691.6 *9*	$\frac{3}{2}$	2684.1 *5*	346 *83*	7.535 $(\frac{5}{2}^+)$		[e]2686 *11*	
			2654.8 *6*	176 *57*	35.844 $(\frac{3}{2}^-)$			
			2599.6 *6*	261 *91*	90.875 $(\frac{5}{2}^-)$			
			2565.5 *5*	314 *78*	126.412 $(\frac{1}{2}^-)$[c]			
			2509.1 *3*	463 *91*	182.902 $(\frac{5}{2}^-)$			
			2286.6 *5*	236 *73*	404.129 $(\frac{1}{2}^-)$[d]			
[x]3169.9 *7*			[x]2293.0 *7*	197 *66*	404.129 $(\frac{1}{2}^-)$[d]			
3168.7 *4*	2699.7 *8*	$\frac{3}{2}$	2692.4 *4*	367 *86*	7.535 $(\frac{5}{2}^+)$			
			2572.8 *3*	623 *103*	126.412 $(\frac{1}{2}^-)$[c]			
			2516.7 *3*	662 *111*	182.902 $(\frac{5}{2}^-)$			
			2378.1 *7*	149 *53*	321.113 $(\frac{3}{2}^+)$			
3158.3 *5*	2710.1 *9*	$\frac{3}{2}$	2619.3 *7*	185 *70*	90.875 $(\frac{5}{2}^-)$		[e]2721 *12*	
			2582.6 *4*	397 *92*	126.412 $(\frac{1}{2}^-)$[c]			
3153.7 *5*	2714.7 *9*	$\frac{1}{2}, \frac{3}{2}$	2679.3 *5*	210 *63*	35.844 $(\frac{3}{2}^-)$		[e]2721 *12*	
			2392.9 *5*	220 *67*	321.113 $(\frac{3}{2}^+)$			
			2309.4 *4*	244 *64*	404.129 $(\frac{1}{2}^-)$[d]			
3145.5 *5*	2722.9 *9*	$\frac{3}{2}$	2722.4 *5*	472 *117*	0 $(\frac{3}{2}^+)$		[e]2721 *12*	
			2714.8 *5*	344 *84*	7.535 $(\frac{5}{2}^+)$			
			2632.6 *6*	208 *74*	90.875 $(\frac{5}{2}^-)$			
			2596.2 *6*	177 *55*	126.412 $(\frac{1}{2}^-)$[c]			
[x]3125.9 *5*			[x]2421.4 *5*	315 *82*	321.113 $(\frac{3}{2}^+)$			
[x]3124.4 *4*			[x]2708.2 *4*	390 *82*	35.844 $(\frac{3}{2}^-)$			
[x]3121.3 *5*			[x]2341.6 *5*	266 *67*	404.129 $(\frac{1}{2}^-)$[d]			
3111.5 *4*	2756.9 *8*	$\frac{1}{2}, \frac{3}{2}$	2629.1 *5*	285 *71*	126.412 $(\frac{1}{2}^-)$[c]		[e]2751 *12*	
			2351.9 *3*	415 *88*	404.129 $(\frac{1}{2}^-)$[d]			
[x]3091.3 *6*			[x]2371.6 *6*	168 *54*	404.129 $(\frac{1}{2}^-)$[d]			
[x]3086.0 *6*			[x]2782.4 *6*	316 *108*	0 $(\frac{3}{2}^+)$			
[x]3082.8 *9*			[x]2464.5 *9*	121 *67*	321.113 $(\frac{3}{2}^+)$			
3079.5 *5*	**2788.9** ***9***	$\frac{3}{2}$	2789.3 *5*	540 *133*	0 $(\frac{3}{2}^+)$		2788 *14*	
			2780.7 *4*	418 *90*	7.535 $(\frac{5}{2}^+)$			
			2752.9 *4*	443 *88*	35.844 $(\frac{3}{2}^-)$			
			2699.0 *6*	257 *81*	90.875 $(\frac{5}{2}^-)$			
			2661.8 *5*	296 *72*	126.412 $(\frac{1}{2}^-)$[c]			
			2605.0 *5*	226 *62*	182.902 $(\frac{5}{2}^-)$			
[x]3067.2 *6*			[x]2618.3 *6*	108 *44*	182.902 $(\frac{5}{2}^-)$			
[x]3063.0 *8*			[x]2797.4 *7*	188 *62*	7.535 $(\frac{5}{2}^+)$			
[x]3061.1 *8*			[x]2716.4 *8*	150 *62*	90.875 $(\frac{5}{2}^-)$			

(Continued.)

Present Work					ENSDF			
E_1	E_i	J_i	E_2	$I_{\gamma\gamma}$	E_f	E_1[a]	E_i[b]	J_i
3056.2 *6*	2812.2 *10*	$\frac{1}{2}, \frac{3}{2}$	2776.0 *5*	175 *58*	35.844 $(\frac{3}{2}^-)$			
			2407.2 *7*	143 *50*	404.129 $(\frac{1}{2}^-)$[d]			
[x]3046.5 *6*			[x]2416.5 *6*	159 *54*	404.129 $(\frac{1}{2}^-)$[d]			
[x]3040.0 *7*			[x]2423.0 *7*	91 *45*	404.129 $(\frac{1}{2}^-)$[d]			
[x]3037.0 *5*			[x]2510.3 *5*	369 *103*	321.113 $(\frac{3}{2}^+)$			
3017.5 *8*	2850.9 *12*	$\frac{1}{2}, \frac{3}{2}$	2529.9 *9*	119 *55*	321.113 $(\frac{3}{2}^+)$			
			2369.8 *7*	199 *91*	481.088 $(\frac{3}{2}^+)$			
3009.6 *7*	2858.8 *11*	$\frac{1}{2}, \frac{3}{2}$	2858.6 *7*	271 *104*	0 $(\frac{3}{2}^+)$			
			2537.9 *7*	157 *63*	321.113 $(\frac{3}{2}^+)$			
[x]3007.2 *4*			[x]2770.4 *4*	409 *99*	90.875 $(\frac{5}{2}^-)$			
[x]2994.6 *5*			[x]2838.0 *5*	294 *75*	35.844 $(\frac{3}{2}^-)$			
[x]2976.2 *6*			[x]2571.1 *6*	186 *63*	321.113 $(\frac{3}{2}^+)$			
2947.0 *7*	2921.4 *11*	$\frac{3}{2}$	2737.8 *6*	235 *75*	182.902 $(\frac{5}{2}^-)$		[e]2912 *14*	
			2441.0 *8*	155 *78*	481.088 $(\frac{3}{2}^+)$			
[x]2943.0 *7*			[x]2604.3 *7*	270 *84*	321.113 $(\frac{3}{2}^+)$			
2937.5 *5*	2930.9 *9*	$\frac{1}{2}, \frac{3}{2}$	2803.8 *5*	306 *72*	126.412 $(\frac{1}{2}^-)$[c]		[e]2944 *14*	
			2609.5 *6*	223 *75*	321.113 $(\frac{3}{2}^+)$			
2928.1 *6*	2940.3 *10*	$\frac{3}{2}$	2932.9 *6*	256 *70*	7.535 $(\frac{5}{2}^+)$		[e]2944 *14*	
			2757.3 *6*	270 *80*	182.902 $(\frac{5}{2}^-)$			
[x]2925.2 *7*			[x]2537.7 *7*	218 *78*	404.129 $(\frac{1}{2}^-)$[d]			
[x]2918.6 *6*			[x]2766.9 *6*	190 *68*	182.902 $(\frac{5}{2}^-)$			
[x]2913.9 *4*			[x]2633.4 *4*	111 *42*	321.113 $(\frac{3}{2}^+)$			
2891.3 *7*	2977.1 *11*	$\frac{3}{2}$	2970.0 *5*	353 *82*	7.535 $(\frac{5}{2}^+)$		[e]2972 *15*	
			2655.7 *7*	228 *89*	321.113 $(\frac{3}{2}^+)$			
			2571.9 *8*	222 *78*	404.129 $(\frac{1}{2}^-)$[d]			
			2495.7 *7*	316 *122*	481.088 $(\frac{3}{2}^+)$			
[x]2887.1 *7*			[x]2660.2 *7*	230 *89*	321.113 $(\frac{3}{2}^+)$			
2881.0 *7*	2987.4 *11*	$\frac{1}{2}, \frac{3}{2}$	2666.7 *7*	174 *65*	321.113 $(\frac{3}{2}^+)$		[e]2994 *15*	
			2581.5 *7*	191 *74*	404.129 $(\frac{1}{2}^-)$[d]			
[x]2876.0 *9*			[x]2809.5 *9*	109 *61*	182.902 $(\frac{5}{2}^-)$			
2870.1 *5*	2998.3 *9*	$\frac{1}{2}, \frac{3}{2}$	2870.6 *4*	192 *40*	126.412 $(\frac{1}{2}^-)$[c]		[e]2994 *15*	
			2593.4 *6*	197 *78*	404.129 $(\frac{1}{2}^-)$[d]			
2852.8 *5*	3015.6 *9*	$\frac{1}{2}, \frac{3}{2}$	2979.3 *3*	1189 *143*	35.844 $(\frac{3}{2}^-)$		[e]3021 *15*	
			2888.7 *6*	237 *69*	126.412 $(\frac{1}{2}^-)$[c]			
2847.1 *5*	**3021.3 *9***	$\frac{1}{2}, \frac{3}{2}$	3021.7 *4*	652 *144*	0 $(\frac{3}{2}^+)$		3021 *15*	
			2893.7 *6*	254 *72*	126.412 $(\frac{1}{2}^-)$[c]			
2835.7 *7*	3032.7 *11*	$\frac{3}{2}$	2941.3 *6*	270 *83*	90.875 $(\frac{5}{2}^-)$		[e]3021 *15*	
			2850.0 *8*	186 *70*	182.902 $(\frac{5}{2}^-)$			
			2712.0 *7*	136 *58*	321.113 $(\frac{3}{2}^+)$			
2829.4 *5*	3039.0 *9*	$\frac{3}{2}$	3003.3 *3*	599 *102*	35.844 $(\frac{3}{2}^-)$		[e]3047 *15*	
			2911.8 *4*	296 *71*	126.412 $(\frac{1}{2}^-)$[c]			
			2855.8 *7*	168 *67*	182.902 $(\frac{5}{2}^-)$			
2815.5 *5*	3052.9 *9*	$\frac{3}{2}$	3052.3 *5*	453 *124*	0 $(\frac{3}{2}^+)$		[e]3047 *15*	
			3017.0 *3*	465 *92*	35.844 $(\frac{3}{2}^-)$			

(Continued.)

Present Work					ENSDF			
E_1	E_i	J_i	E_2	$I_{\gamma\gamma}$	E_f	E_1[a]	E_i[b]	J_i
			2870.8 *6*	245 *83*	182.902 $(\frac{5}{2}^-)$			
2791.3 *5*	3077.1 *9*	$\frac{1}{2}, \frac{3}{2}$	3040.9 *3*	392 *85*	35.844 $(\frac{3}{2}^-)$		[e]3073 *15*	
			2950.1 *6*	139 *50*	126.412 $(\frac{1}{2}^-)$[c]			
[x]2778.3 *3*			[x]2684.6 *3*	203 *45*	404.129 $(\frac{1}{2}^-)$[d]			
[x]2758.2 *7*			[x]2704.7 *7*	119 *41*	404.129 $(\frac{1}{2}^-)$[d]			
2740.5 *4*	3127.9 *8*	$\frac{1}{2}, \frac{3}{2}$	3127.4 *4*	687 *141*	0 $(\frac{3}{2}^+)$		[e]3135 *12*	
			3092.6 *4*	338 *77*	35.844 $(\frac{3}{2}^-)$			
2696.4 *5*	3172.0 *9*	$\frac{1}{2}, \frac{3}{2}$	3171.5 *4*	545 *121*	0 $(\frac{3}{2}^+)$		[e]3187 *16*	
			3136.3 *7*	135 *51*	35.844 $(\frac{3}{2}^-)$			
			2851.2 *7*	237 *78*	321.113 $(\frac{3}{2}^+)$			
			2766.8 *4*	218 *51*	404.129 $(\frac{1}{2}^-)$[d]			
2622.4 *6*	3246.0 *10*	$\frac{1}{2}, \frac{3}{2}$	3210.2 *6*	168 *51*	35.844 $(\frac{3}{2}^-)$		[e]3253 *16*	
			3118.5 *5*	341 *77*	126.412 $(\frac{1}{2}^-)$[c]			
			2925.2 *7*	187 *63*	321.113 $(\frac{3}{2}^+)$			
2587.0 *5*	3281.4 *9*	$\frac{3}{2}$	3274.5 *6*	195 *62*	7.535 $(\frac{5}{2}^+)$		[e]3268 *16*	
			3245.5 *5*	206 *56*	35.844 $(\frac{3}{2}^-)$			
			3153.5 *5*	329 *85*	126.412 $(\frac{1}{2}^-)$[c]			
2579.8 *5*	3288.6 *9*	$\frac{1}{2}, \frac{3}{2}$	3252.8 *4*	317 *70*	35.844 $(\frac{3}{2}^-)$		[e]3291 *12*	
			2967.5 *6*	194 *66*	321.113 $(\frac{3}{2}^+)$			
2563.2 *5*	3305.2 *9*	$\frac{3}{2}$	3269.4 *4*	297 *66*	35.844 $(\frac{3}{2}^-)$		[e]3316 *16*	
			3122.4 *6*	120 *46*	182.902 $(\frac{5}{2}^-)$			
2554.5 *4*	3313.9 *8*	$\frac{1}{2}, \frac{3}{2}$	3277.5 *3*	515 *86*	35.844 $(\frac{3}{2}^-)$		[e]3316 *16*	
			2993.4 *6*	269 *85*	321.113 $(\frac{3}{2}^+)$			
2549.2 *7*	3319.2 *11*	$\frac{3}{2}$	3319.7 *6*	284 *85*	0 $(\frac{3}{2}^+)$		[e]3316 *16*	
			3312.2 *7*	142 *50*	7.535 $(\frac{5}{2}^+)$			
			2912.8 *7*	189 *73*	404.129 $(\frac{1}{2}^-)$[d]			
2527.2 *5*	3341.2 *9*	$\frac{3}{2}$	3334.3 *6*	115 *43*	7.535 $(\frac{5}{2}^+)$		[e]3349 *12*	
			3305.6 *5*	269 *63*	35.844 $(\frac{3}{2}^-)$			
			3157.4 *5*	204 *63*	182.902 $(\frac{5}{2}^-)$			
2514.3 *7*	3354.1 *11*	$\frac{1}{2}, \frac{3}{2}$	3354.0 *8*	161 *70*	0 $(\frac{3}{2}^+)$		[e]3349 *12*	
			3225.9 *6*	227 *62*	126.412 $(\frac{1}{2}^-)$[c]			
			2948.6 *9*	134 *64*	404.129 $(\frac{1}{2}^-)$[d]			
2508.0 *7*	**3360.4 *11***	$\frac{3}{2}$	3270.0 *6*	255 *85*	90.875 $(\frac{5}{2}^-)$		3361 *12*	
			2954.4 *7*	197 *76*	404.129 $(\frac{1}{2}^-)$[d]			
2446.3 *6*	3422.1 *10*	$\frac{1}{2}, \frac{3}{2}$	3294.5 *5*	187 *50*	126.412 $(\frac{1}{2}^-)$[c]		[e]3414 *15*	
			3017.6 *6*	187 *58*	404.129 $(\frac{1}{2}^-)$[d]			
			2940.3 *8*	146 *74*	481.088 $(\frac{3}{2}^+)$			
[x]2428.1 *7*			[x]3119.7 *8*	161 *60*	321.113 $(\frac{3}{2}^+)$			
2333.0 *5*	3535.4 *9*	$\frac{1}{2}, \frac{3}{2}$	3500.1 *6*	237 *66*	35.844 $(\frac{3}{2}^-)$			
			3407.7 *3*	337 *67*	126.412 $(\frac{1}{2}^-)$[c]			

(Continued.)

Present Work					ENSDF			
E_1	E_i	J_i	E_2	$I_{\gamma\gamma}$	E_f	E_1[a]	E_i[b]	J_i
2104.7 *6*	3763.7 *10*	$\frac{1}{2}, \frac{3}{2}$	3763.3 *5*	232 *78*	0 $(\frac{3}{2}^+)$		[e]3759 *13*	
			3443.0 *7*	103 *46*	321.113 $(\frac{3}{2}^+)$			

[a]Data taken from the (n, γ) with thermal and 2-keV neutron datasets in Ref. [6].
[b]Data taken from the Adopted Level dataset in Ref. [6].
[c]Unresolved final levels: 126.412 $(\frac{1}{2}^-)$ or 127.298 $(\frac{3}{2}^-)$.
[d]Unresolved final levels: 404.129 $(\frac{1}{2}^-)$ or 405.470 $(\frac{3}{2}^-)$.
[e]Energy of the observed level, which agrees with those obtained from the ion-induced ^{152}Sm(d, p) and/or $^{154}(p, d)$ and/or $^{154}(d, t)$ reactions within their uncertainty. It is noted that the superscript denotation "e" is not marked if the discrepancy between the observed level and that presented in the ENSDF library is less than 1.5 keV.
[f]The values of the 630.20-keV level and its spin are taken from the (n, γ) experiments.
[g]The spin value of $\frac{1}{2}\hbar$ was assigned to the 695.80-keV level in the ENSDF library based on the strong supports from the l transfer and vector analyzing power in the (d, t) particle-transfer reaction, whereas the present work suggests a different spin value, namely $\frac{3}{2}\hbar$. Our suggestion for this level is made based on its weak 604.8-keV dipole transition to the 90.875-keV $(\frac{5}{2}^-)$ state. In the case where the 604.8-keV transition is quadrupole, the spin of $\frac{1}{2}\hbar$ must be assigned to the 695.7-keV level found within the present work.
[h]This level cannot be distinguished from the 734.7 keV $(\frac{1}{2}^+)$ level within the present experiment.
[i]This level cannot be distinguished from the 984.3 keV $(\frac{3}{2}^-)$ level within the present experiment.
[j]The observed levels of 2494.7 *10* and 2497.1 *9* keV both agree with the 2496.6 *12* keV state within their experimental uncertainties. Thus, there is a possibility that these three levels are all the same.
[x]The γ cascades, which we are not able to identify as the primary transitions within the present work.

as the primary ones despite that they appear in only one TSC spectrum because these transitions are found to be the same as the primary transitions that currently exist in the ENSDF library [6].

Since the compound state of ^{153}Sm has the spin of $\frac{1}{2}\hbar$, by using Eq. (1) together with an assumption that all the observed transitions are dipole, we are able to tentatively assign a unique spin value of $\frac{3}{2}\hbar$ for 53 intermediate levels, which correspond to the γ transitions emitted from the compound state to 3 final levels with the spins of $\frac{5}{2}\hbar$, namely the 7.535 $(\frac{5}{2}^+)$, 90.875 $(\frac{5}{2}^-)$, and 182.902 $(\frac{5}{2}^-)$ keV levels. For the remaining 50 levels, which relate to the γ transitions emitted from the compound state to the final levels with the spin of $\frac{1}{2}\hbar$ or $\frac{3}{2}\hbar$, their spin values cannot be uniquely deduced. Consequently, a possible spin range from $\frac{1}{2}\hbar$ to $\frac{3}{2}\hbar$ has tentatively been assigned to these levels.

The assumption that all the observed transitions are dipole is made based on the following experimental evidence. First, among all the transitions coming from the compound state (see the (n, γ) datasets for thermal and 2-keV neutrons in Ref. [6]), we found only two transitions which are not dipole, namely the 5506.4- and 5861.4-keV transitions to the 362.286 $(\frac{5}{2}^+)$ and 7.535 $(\frac{5}{2}^+)$ keV levels, respectively. These transitions, however, have considerably low intensities compared to other primary transitions. Moreover, the 5506.4-keV transition was solely found in Ref. [1], whereas that of 5861.4 keV was only detected in the form of a doublet with the strong transition of 5868.4 keV in Refs. [1,5,21], and has not been reproduced within the framework of the (n, γ) experiment with 2-keV neutron [17]. Second, within the low-excitation energy of ^{153}Sm level scheme, the quadrupole transitions have rarely been reported. In fact, there are only few quadrupole transitions, which currently exist in the ENSDF library, such as the 223.173- and 278.17-keV transitions coming from the 276.713- and 405.470-keV levels, respectively. They all together have lower energy than the energy threshold of the present work (520 keV for both transition and excitation energy). This evidence apparently ensures the validity of the assumption above and consequently the reliability of the spin assignment within the present work. Nevertheless, the assumption is still restrictive and thus the spin assignment within the present work can not be determined as a definite value.

By comparing the ^{153}Sm level scheme obtained within the present work with that extracted from the ENSDF library [6], we have realized that 29 primary γ transitions and 42 intermediate levels are found to be the same within their uncertainties, whereas only 8 secondary transitions are the same with those existed in the ENSDF library. The remaining 74 primary γ transitions, 61 intermediate levels, and 291 secondary transitions are therefore considered as the new data obtained within the present experiment.

In particular, the ^{153}Sm level scheme obtained within the present work agrees well with that obtained within the previous studies using the same ^{152}Sm(n_{th}, γ) reaction [1,5,17,21]. For the energy region below 5300 keV, which is the maximum γ energy that can be detected within the present experiment (because the energy threshold of detectors were set to be around 520 keV), we have reproduced 19 over 24 primary transitions that were previously reported in Refs. [1,5,17,21]. Among the 5 unreproduced transitions, 2 transitions, whose energies are 5220.4 and 5283.9 keV, were reported in Ref. [5], whereas 2 transitions with the energies of 4850 and 4864.0 keV were detected in Ref. [1]. These transitions were found a very long time ago and have not been

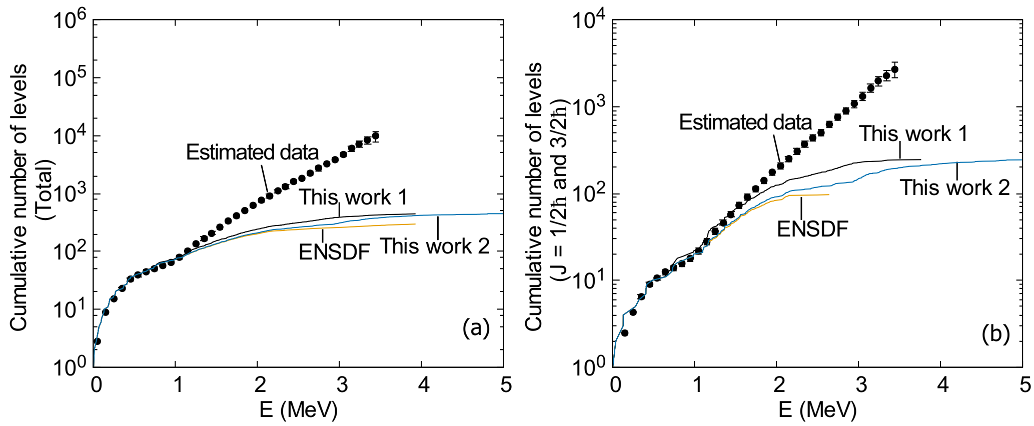

FIG. 4. Total (a) and partial (b) cumulative numbers of levels obtained by using the NLD data in Ref. [29] (estimated data) and ENSDF data in Ref. [6] in comparison with those taken from "this work 1" and "this work 2" (see the explanation in the text).

reproduced by other experiments. The remaining 4505.6-keV transition was reported with a slightly different energy of 4506.6 ± 1.0 keV in Ref. [21], 4505.8 ± 0.4 keV in Ref. [5], or 4506.5 ± 0.6 keV in Ref. [1]. This 4505.6-keV transition might therefore be the same as the 4507.4 ± 0.4 keV transition observed within the present work as well as the 4507.41-keV transition obtained from the (n, γ) experiment with the 2-keV neutron source in Ref. [17]. In general, we have reproduced 22 over 26 levels that were reported by the previous (n_{th}, γ) experiments within the excitation energy above 600 keV in Refs. [1,5,17,21].

The result of the ^{153}Sm level scheme obtained within the present work also agrees well with the neutron-capture experiment using 2-keV neutron source; namely, 22 over 24 primary transitions within the γ energy of 520 to 5300 keV and 23 over 29 levels within the excitation energy region of 600 to 2000 keV reported in Ref. [17] have been replicated within the present experiment. Among the remaining unreproduced levels, 4 levels, whose energies are 1675.8, 1723.5, 1737.5, and 1751.4 keV, have been determined in Ref. [17] without any populating γ transitions. In addition, all the levels reported in Ref. [17] with the assigned spins of $\frac{1}{2}\hbar$ or $\frac{3}{2}\hbar$ are in full agreement with those deduced from the present study.

Furthermore, our data also go along with those obtained within the ion-induced experiments, in particular the ^{152}Sm(d, p) [15–17], $^{154}(p, d)$ [17,18], and $^{154}(d, t)$ [5,16,17] reactions. Below 2000 keV, 24 excited levels found in the present work are supported by at least one of the experiments employing the ion-induced reactions. Similarly, 44 excited levels found within the present experiment agree with those extracted from the ion-induced reactions within their uncertainties (see the excited levels with the superscript denotation "e" in Table II). It should be noted here that the uncertainties of the data obtained within the ion-induced experiments are often in the range of 8 to 18 keV, which are much larger than those obtained within the present work. Therefore, we consider that two levels are the same only if their discrepancy is less than 1.5 keV; that is, if a level deduced from the present experiment agrees with that deduced from the ion-induced experiments but the discrepancy between the two levels is larger than 1.5 keV, it is considered as the new level.

Table II presents the absolute intensities normalized to 10^6 captures together with the statistical uncertainties of all 386 measured cascades. The normalization factor is determined based on the absolute intensities of 4697.2- and 5117.8-keV primary transitions (i.e., the 4697.4- and 5118.3-keV transitions within the present work) taken from the ENSDF data [6] together with their branching ratios. The latter are determined from the gating spectrum of the primary transitions mentioned above. Since the energy threshold of the present experiment is 520 keV, we are not able to identify the branches, whose energy of the secondary transition is less than 520 keV. Therefore, our cascade intensities may contain a certain systematic error.

In general, the present experiment reproduces most of the ENSDF data obtained from the neutron-capture and ion-induced reactions. This consistency obviously proves the reliability of the data obtained within the present study.

Thanks to the coincidence technique, the influence of ^{150}Sm on the spectroscopic information of ^{153}Sm, which limits the number of data obtained from the neutron-capture experiment using the conventional HPGe detector [1,5,21], has been considerably reduced within the present experiment. This technique also reduces the peak overlaps, which are immensely common in analyzing the conventional prompt γ spectra, especially for nuclei with the complicated level scheme such as ^{153}Sm. The reason is that the coincidence technique is able to detect only the intermediate level in a narrow spin range from $J_i - 1$ to $J_i + 1$ (J_i is the spin of the compound state) and the detected γ transitions are distributed to the multiple TSC spectra. As a result, we are able to detect more important information on the level scheme of ^{153}Sm, which does not currently exist in the ENSDF library.

B. Cumulative number of levels

1. Experimental cumulative number of levels

Since several new energy levels have been detected in the present experiment, we are able to construct the total and partial cumulative numbers of levels, which are, by definition, the numbers of excited levels falling within the specific energy and spin ranges. These cumulative numbers are constructed

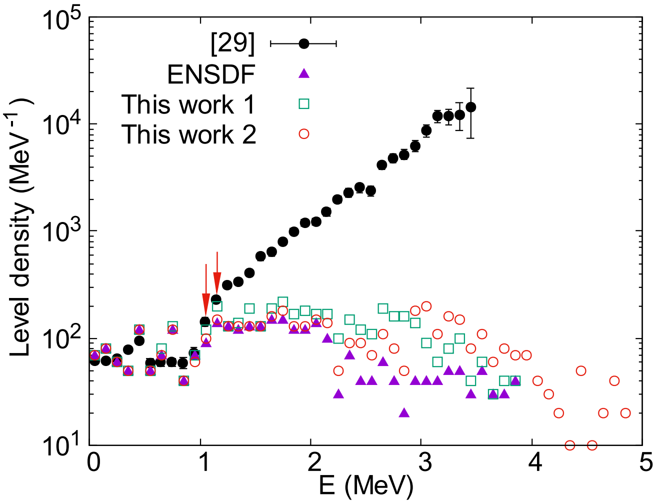

FIG. 5. Total level density obtained by counting the numbers of discrete levels in the ENSDF, "this work 1" and "this work 2," vs the NLD data taken from Ref. [29].

by combining the adopted levels taken from the ENSDF [6] with those obtained within the present work (Table II). For the latter, however, there are unassigned intermediate levels corresponding to 87 γ cascades as shown in Table II with the superscript denotation "x." Therefore, we have constructed two cumulative curves denoted as "this work 1" and "this work 2" (see Fig. 4). "This work 1" is created by assuming that the γ transitions in each of 87 cascades with the higher energies are considered as the primary transitions, whereas those with lower energies correspond to the secondary ones. "This work 2" is generated by using the opposite assumption, namely that the γ transitions with lower (higher) energies are considered as the primary (secondary) ones. It is obvious that "this work 1" is always higher than "this work 2," regardless of their total or partial cumulative curves because "this work 1" contains the primary γ transitions, whose energies are higher than those in "this work 2" (Fig. 4). Here, it should be noted that the assumption for "this work 1" should be much more reliable than that for "this work 2" because within the two-step cascades, one often observes the primary transition, whose energy is higher than that of the secondary one (see, e.g., the data reported in the ENSDF library [7]). Consequently, the real cumulative curve should probably be very close to "this work 1."

The total and partial cumulative numbers of levels within the present work are also compared with those obtained by using the NLD data in Ref. [29]. The total cumulative curve in this case is calculated by using the conventional formula [30]

$$N(E_x) = \int_0^{E_x} \rho(E)dE \, , \tag{2}$$

where $\rho(E)$ is the experimental NLD taken from Ref. [29]. As for the partial cumulative curve for the spin range $J = [\frac{1}{2}, \frac{3}{2}]\hbar$, it should be calculated using the same Eq. (2) but the J-dependent NLD $\rho(E,J)$ must be used instead of the total NLD $\rho(E)$. However, there exists in literature only the total NLD extracted by using the Oslo method $\rho(E)$ in Ref. [29]. The latter was extracted from the γ spectra of the ^{154}Sm$(p,d\gamma)^{153}$Sm reaction and was later normalized using the discrete levels taken from the ENSDF library [7] as well as the NLD data at the neutron binding energy (see, e.g., Fig. 3 of Ref. [29]). Therefore, in order to estimate the $\rho(E,J)$ values, we have multiplied $\rho(E)$ with a factor, which is determined as the ratio between the number of levels with spins $J = \frac{1}{2}$ and $\frac{3}{2}\hbar$ and the total number of levels existed in the ENSDF library [6]. This factor is found to be about 0.27 for ^{153}Sm. The obtained $\rho(E,J)$ is then used to calculate the partial cumulative curve $N(E_x, J)$ for $J = [\frac{1}{2}, \frac{3}{2}]\hbar$. For the sake of simplicity, the corresponding results, namely the total and partial cumulative curves estimated using the NLD data in Ref. [29], are called the estimated data or curves hereafter. It is seen in Figs. 4(a) and 4(b) that such an estimation seems

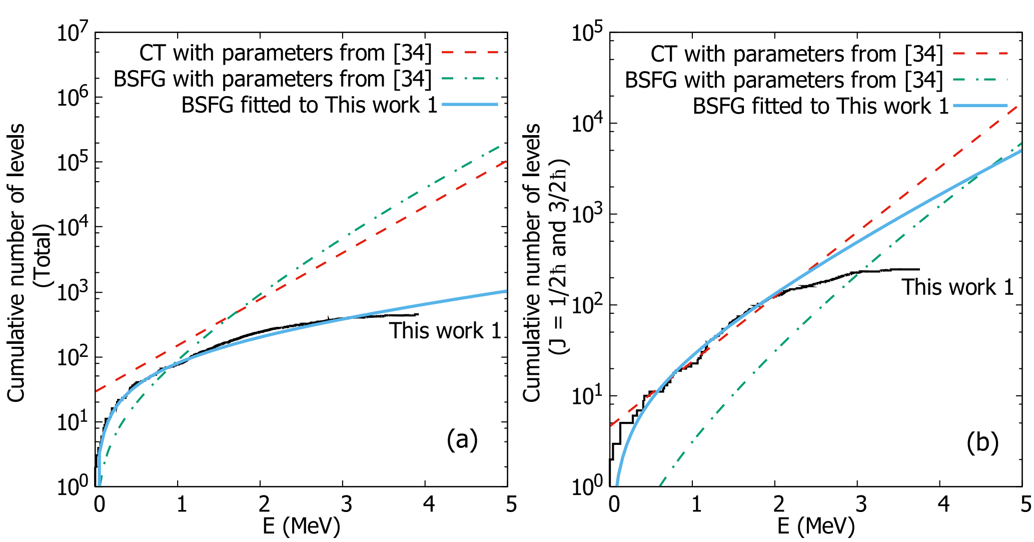

FIG. 6. Comparison between the experimental total (a) and partial (b) cumulative numbers of levels and those predicted by two phenomenological NLD models.

TABLE III. Values of the free parameters obtained within the CT and BSFG models presented in Fig. 6.

Model	CT		BSFG	
Parameter	E_0 (MeV)	T (MeV)	a (MeV^{-1})	E_1 (MeV)
Parameters from Ref. [34]	-2.06 ± 0.29	0.61 ± 0.03	17.76 ± 0.28	-1.08 ± 0.13
Fitted to This work 1 in Fig. 6(a)			3.51 ± 0.28	-12.09 ± 1.24
Fitted to This work 1 in Fig. 6(b)			12.73 ± 0.16	-3.49 ± 0.07

to be valid for the low-energy region (below 1 MeV) as both estimated curves for the total and partial cumulative numbers of levels are in excellent agreement with the ENSDF data. It is obvious that the spin distribution is not constant over the excitation energy. Thus, the estimated data presented in Fig. 4(b) may not be corrected in the high-energy region above 1 MeV. Since the spin distribution changes very slightly when the excitation energy is low, we believe that our deduction is acceptable with a negligible error for the energy region from 1 to 2 MeV. It is interesting to see in Fig. 4(b) that "this work 1" almost coincides with the estimated data in the energy region from 0 to about 1.8 MeV, above which the data obtained from our estimation might no longer be valid. On the other hand, "this work 2" and ENSDF curves agree with the estimated data up to about 1 MeV only. This result strongly supports the validity of the assumption for "this work 1," which is the most common assumption used in the two-step cascade experiments, as explained above. This assumption can also be confirmed by comparing the total NLD in Ref. [29] with those obtained from the ENSDF, "this work 1," and "this work 2" (Fig. 5). It is clear to see in Fig. 5 that the total NLDs taken from the ENSDF and "this work 2" only agree with the data of Ref. [29] below 1 MeV, whereas the agreement between the data from "this work 1" and Ref. [29] is extended up to about 1.2 MeV, indicated by two arrows in Fig. 5.

The results obtained from "this work 1" as shown in Figs. 4 and 5 indicate two significant contributions of the new levels found within the present work. The first contribution is that for the total NLD, the maximum excitation energy $E_{\max}$, defined as the energy threshold below which most of the excited levels have been observed, is now extended to about 1.2 MeV, instead of 1.0 MeV, as had been obtained from the ENSDF data [6] [Figs. 4(a) and 5]. The second contribution is associated with the value of $E_{\max}$ for the spin range of $[\frac{1}{2}, \frac{3}{2}]\hbar$, which has been increased up to about 1.8 MeV [Fig. 4(b)]. It is evident that the NLD calculated by counting the numbers of discrete levels has been widely considered as the most reliable data, and often used for the normalization of the experimentally extracted data [24] as well as different NLD model calculations [31,32]. However, the present ENSDF library provides reliable NLD up to about 1 MeV only. By including our new data, we are able to obtain reliable NLD data up to about 1.2 and 1.8 MeV for the total and partial (within the spin range of $[\frac{1}{2}, \frac{3}{2}]\hbar$) NLDs, respectively. This second contribution is therefore the most important contribution of the present work.

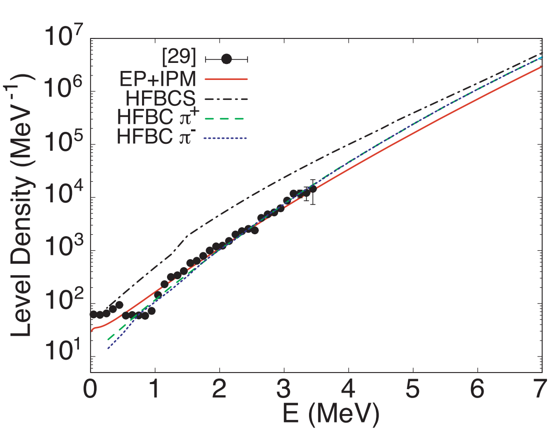

FIG. 7. Comparison between the total NLDs obtained within different microscopic NLD models and the experimental data taken from Ref. [29].

2. Comparison with theoretical models

The cumulative number of levels is very helpful for verifying the predictive power of the NLD models. In Fig. 6, we compare our experimental cumulative curve (this work 1) with two phenomenological NLD models, namely the back-shifted Fermi gas (BSFG) and constant temperature (CT). The functional forms of these two models are taken from Ref. [33], that is,

$$\rho_{\rm CT}(E,J) = f(J)\rho_{\rm CT}(E) = f(J)\frac{1}{T}e^{(E-E_0)/T}, \quad (3)$$

$$\rho_{\rm BSFG}(E,J) = f(J)\rho_{\rm BSFG}(E) = f(J)\frac{e^{2\sqrt{a(E-E_1)}}}{12\sqrt{2}\sigma a^{1/4}(E-E_1)^{5/4}}, \quad (4)$$

$$f(J) = e^{-J^2/2\sigma^2} - e^{-(J+1)^2/2\sigma^2} \simeq \frac{2J+1}{2\sigma^2}e^{-(J+\frac{1}{2})/2\sigma^2}, \quad (5)$$

where $\sigma_{\rm CT} = 0.98A^{0.29}$ and $\sigma_{\rm BSFG} = 0.0146A^{5/3}\frac{1+\sqrt{1+4a(E-E1)}}{2a}$ are the spin cut-off parameters with E_1 and a being the back-shifted energy and level density parameters, respectively. Two parameters E_0 and T in Eq. (3) are the energy shift and constant temperature, whereas the function $f(J)$ in Eq. (5) is the conventional spin distribution of the NLD [30]. The free parameters a, E_1, E_0, and T of the BSFG and CT are often adjusted to fit the total cumulative number of levels as well as the NLD determined from the experimentally averaged neutron-resonance spacing data (D_0 value) [34]. The values of these free parameters taken from Ref. [34] (see also Table III) were used to calculate $\rho_{\rm CT}(E)$, $\rho_{\rm BSFG}(E)$, $\rho_{\rm CT}(E,J)$, and $\rho_{\rm BSFG}(E,J)$ ($J = [\frac{1}{2}, \frac{3}{2}]\hbar$). The total and J-dependent cumulative numbers of levels are then

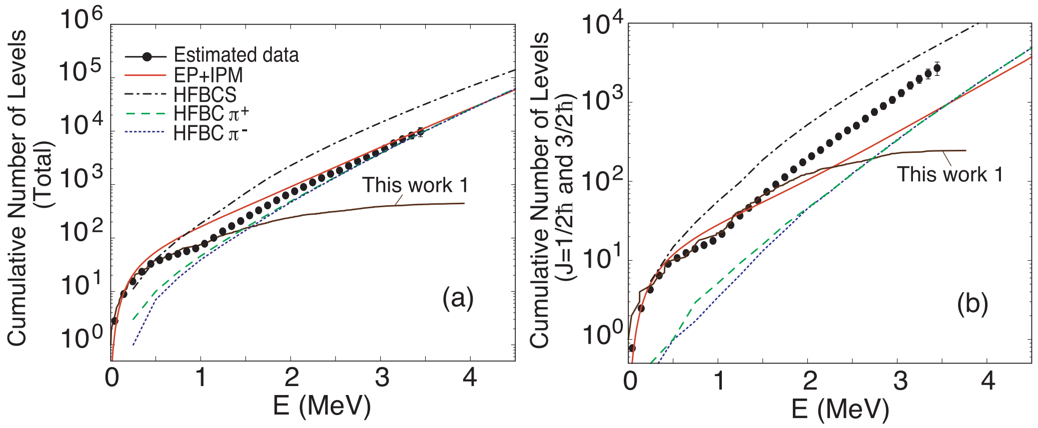

FIG. 8. Total (a) and partial (b) cumulative numbers of levels obtained within different microscopic NLD models in comparison with the experimental data obtained within the present work (this work 1) and those calculated from the experimental NLD data in Ref. [29] (estimated data).

calculated making use of Eq. (2). The results obtained shown in Fig. 6(b) indicate that the CT model with parameters taken from Ref. [34] fits well to our experimental data (this work 1) for the spin range of $[\frac{1}{2}, \frac{3}{2}]\hbar$, but it is higher than our experimental total cumulative curve [Fig. 6(a)]. The reason is that the parameters of the CT model taken from Ref. [34] were given based on the analysis of 21 excited levels below 0.49 MeV within the spin range of $[\frac{1}{2}, \frac{9}{2}]\hbar$ (close to the spin range of $[\frac{1}{2}, \frac{3}{2}]\hbar$ within the present work), whereas below 0.49 MeV, there must be in total 37 excited levels within a much larger spin range of $[\frac{1}{2}, \frac{19}{2}]\hbar$ as in the ENSDF library [6]. Consequently, while the CT model describes well the experimental J-dependent cumulative curve, it is unable to describe the total one. For the BSFG model with the free parameters taken from the same Ref. [34], it completely fails to describe both the total and J-dependent experimental cumulative curves (see Fig. 6). The above results of the CT and BSFG models clearly demonstrate that the prediction of the phenomenological NLD models depends strongly on the values of their free parameters. For instance, by refitting the results of the BSFG model to our total and J-dependent experimental cumulative data, we obtain the different sets of free parameters as reported in Table III. To obtain reliable predicting power, one should therefore use the microscopic NLD models instead of the phenomenological ones.

Within the present paper, three microscopic NLD models have been selected, namely the Hartree-Fock BCS (HFBCS) [31], the Hartree-Fock-Bogoliubov plus combinatorial method (HFBC) for the positive (HFBC π^+) and negative (HFBC π^-) parities [32], and the recent exact pairing plus independent-particle model at finite temperature (EP+IPM) [35]. The HFBCS and HFBC data are accessible from RIPL-2 [36] and RIPL-3 [37], respectively. These models have been considered to be the most up-to-date microscopic theoretical models for the NLD. Figure 7 shows the total NLD $\rho(E)$ obtained within the HFBCS, HFBC, and EP+IPM in comparison with the experimental data. This figure indicates that while the HFBCS agrees with the experimental data only in the very low-energy region (below 0.5 MeV), both the HFBC and EP+IPM offer a good fit to the measured data. Moreover, the HFBC cannot describe the data below 0.5 MeV, whereas the EP+IPM, in general, agrees with both low- and high-energy data. Consequently, one can easily see in Fig. 8 that only the EP+IPM can describe both the experimental total and partial cumulative curves. This result of EP+IPM does not go beyond our expectation because this model has successfully been used to describe the NLD data of not only hot $^{170-172}$Yb [35] and $^{60-62}$Ni [38] nuclei but also several hot rotating $A \sim 200$ isotopes [39]. In addition, the EP+IPM does not use any fitting parameters as discussed in Refs. [35,39,40], whereas the HFBCS and HFBC often employ some fitting coefficients (see, e.g., Eqs. (17) and (18) of Ref. [31] or Eq. (25) of Ref. [32]) to the experimental total cumulative data at low energy and the D_0 value at energy $E = B_n$. The above results, once again, confirm the microscopic nature and universality of the EP+IPM NLD model proposed in Ref. [35]. In other words, the presently updated data provide a good test for both phenomenological and microscopic NLD models.

IV. CONCLUSION

The present paper studies the excited levels of ^{153}Sm nucleus populated in the thermal neutron-capture reaction using the γ-γ coincidence technique and high-resolution HPGe detectors. The coincidence technique together with the highly enriched target for the ^{152}Sm isotope allow us to significantly eliminate the influence of the ^{150}Sm excited nucleus on the observed γ spectrum. In addition, the statistics of the measured data are rather high within the framework of coincident measurements. As a result, we are able to detect many new energy levels and their corresponding γ transitions, namely 74 primary γ transitions, 61 intermediate levels, and 291 secondary transitions. The tentative spin value of 53 observed levels is found to be $\frac{3}{2}\hbar$, whereas the remain levels are tentatively adopted to be in the spin range of $[\frac{1}{2}, \frac{3}{2}]\hbar$.

By combining the updated energy levels with those obtained from the ENSDF library, we have constructed new total and partial (within the spin range of $[\frac{1}{2}, \frac{3}{2}]\hbar$) cumulative numbers of levels and compared the obtained data with those calculated from the experimental NLD data extracted using the Oslo method (estimated data) as well as the predictions of different phenomenological and microscopic NLD models. The good agreement between our cumulative curves with the estimated data allows us to deduce the values of the maximum excitation energy $E_{\max}$, which is defined as the energy threshold below which most of the excited levels have been observed, to be around 1.2 and 1.8 MeV for the total and partial (spins of $[\frac{1}{2}, \frac{3}{2}]\hbar$) NLD data, respectively. These values of $E_{\max}$ are higher than the corresponding values obtained using the present data in the ENSDF library. Moreover, the newly constructed cumulative curves also agree well with the recent microscopic exact pairing plus independent-particle model at finite temperature in which no fitting parameter has been employed.

All the results obtained in the present work are important as they provide updated information on the nuclear level structure and make a step toward the completed level schemes of excited compound nuclei.

ACKNOWLEDGMENTS

N.N.A., N.X.H., P.D.K., H.H.T., and N.Q.H. acknowledge support by the National Foundation for Science and Technology Development (NAFOSTED) of Vietnam through Grant No. 103.04-2017.323. They would also like to thank the Ministry of Science and Technology of Vietnam for the financial support through the project coded KC05.08/16-20. Sincere thanks are given to Prof. Vuong Huu Tan and Prof. Nguyen Nhi Dien for their support and implementation of the neutron beams at Dalat Nuclear Research Reactor, which have been continuously used for the nuclear structure study in Vietnam.

[1] R. K. Smither, E. Bieber, T. von Egidy, W. Kaiser, and K. Wien, Phys. Rev. **187**, 1632 (1969).
[2] J. Rekstad, M. Guttormsen, T. Engeland, G. Løvhøiden, O. Straume, J. Lien, and C. E. Ellegaard, Nucl. Phys. A **320**, 239 (1979).
[3] E. Y. Lure, L. K. Peker, and P. T. Prokof'ev, Izv. Akad. Nauk SSSR, Ser. Fiz. **32**, 74 (1968) [Bull. Acad. Sci. USSR, Phys. Ser. **32**, 74 (1969)].
[4] R. A. Kenefick and R. K. Sheline, Phys. Rev. **135**, B939 (1964).
[5] M. J. Bennett, R. K. Sheline, and Y. Shida, Nucl. Phys. A **171**, 113 (1971).
[6] R. G. Helmer, Nucl. Data Sheets. **107**, 507 (2006).
[7] https://www-nds.iaea.org/public/ensdf_pgm/
[8] M. B. Kime, Ph.D. thesis, Cornell University, Ithaca, New York, United States, 1971.
[9] A. B. MacFarland, Ph.D. thesis, University of Idaho, Moscow, Idaho, United States, 1983.
[10] R. C. Greenwood, M. H. Putnam, and K. D. Watts, Nucl. Inst. Meth. Phys. Res. A **356**, 385 (1995).
[11] R. C. Greenwood, R. G. Helmer, M. H. Putnam, and K. D. Watts, Nucl. Inst. Meth. Phys. Res. A **390**, 95 (1997).
[12] S. J. Asztalos, I. Y. Lee, K. Vetter, B. Cederwall, R. M. Clark, M. A. Deleplanque, R. M. Diamond, P. Fallon, K. Jing, L. Phair *et al.*, Phys. Rev. C **60**, 044307 (1999).
[13] T. Hayakawa, M. Oshima, Y. Hatsukawa, J. Katakura, H. Limura, M. Matsuda, N. Shinohara, Y. Toh, S. Mitarai, T. Shizuma *et al.*, Eur. Phys. J. A **9**, 153 (2000).
[14] D. G. Burke and I. G. Nowikow, Nucl. Phys. A **756**, 308 (2005).
[15] R. A. Kenefick and R. K. Sheline, Phys. Rev. **139**, B1479 (1965).
[16] I. Kaneström and P. O. Tjöm, Nucl. Phys. A **179**, 305 (1972).
[17] A. Gollwitzer, *Studie des deformierten Kernes* ^{153}*Sm mittels Transfer und (n, γ)* (Herbert Utz Verlag, 1997).
[18] N. Blasi, S. Micheletti, M. Pignanelli, R. De Leo, A. Gollwitzer, S. Deylitz, B. D. Valnion, G. Graw, and L. A. Malov, Nucl. Phys. A **624**, 433 (1997).
[19] J. R. Lien, G. Lovhoiden, J. Rekstad, A. Henriques, C. Gaarde, J. S. Larsen, and S. Y. Van Der Werf, Nucl. Phys. A **412**, 92 (1984).
[20] H. E. Martz, R. G. Lanier, G. L. Struble, L. G. Mann, R. K. Sheline, and W. Stoffl, Nucl. Phys. A **439**, 299 (1985).
[21] E. R. Reddingius and H. Postma, Phys. (Amsterdam, Neth.) **40**, 567 (1969).
[22] S. T. Boneva, E. V. Vasil'eva, Y. P. Popov, A. M. Sukhovoi, and V. A. Khitrov, Fiz. Elem. Chastits At. Yadra **22**, 479 (1991) [Sov. J. Part. Nucl. **22**, 232 (1991)].
[23] N. N. Anh, N. X. Hai, P. D. Khang, N. Q. Hung, and H. H. Thang, Nucl. Phys. A **964**, 55 (2017).
[24] A. Schiller, L. Bergholt, M. Guttormsen, E. Melby, J. Rekstad, and S. Siem, Nucl. Instr. Meth. Phys. Res. Sec. A **447**, 498 (2000).
[25] S. F. Mughabghab, *Atlas of Neutron Resonances*, 6th ed. (Elsevier Science, 2018).
[26] M. Wang, G. Audi, F. G. Kondev, W. J. Huang, S. Naimi, and Xing Xu, Chin. Phys. C **41**, 030003 (2017).
[27] A. M. Sukhovoj and V. A. Khitrov, Instrum. Exp. Tech. **27**, 1071 (1984).
[28] J. M. Blatt and V. F. Weisskopf, *Theoretical Nuclear Physics* (Springer-Verlag, New York, 1991).
[29] A. Simon, M. Guttormsen, A. C. Larsen, C. W. Beausang, P. Humby, J. T. Burke, R. J. Casperson, R. O. Hughes, T. J. Ross, J. M. Allmond *et al.*, Phys. Rev. C **93**, 034303 (2016).
[30] A. Gilbert and A. G. W. Cameron, Can. J. Phys. **43**, 1446 (1965).
[31] P. Demetriou and S. Goriely, Nucl. Phys. A **695**, 95 (2001).
[32] S. Goriely, S. Hilaire, and A. J. Koning, Phys. Rev. C **78**, 064307 (2008).
[33] T. von Egidy, H. H. Schmidt, and A. N. Behkami, Nucl. Phys. A **481**, 189 (1988).
[34] T. von Egidy and D. Bucurescu, Phys. Rev. C **72**, 044311 (2005).
[35] N. Q. Hung, N. D. Dang, and L. T. Quynh Huong, Phys. Rev. Lett. **118**, 022502 (2017).
[36] https://www-nds.iaea.org/RIPL-2/
[37] https://www-nds.iaea.org/RIPL-3/
[38] N. D. Dang, N. Q. Hung, and L. T. Quynh Huong, Phys. Rev. C **96**, 054321 (2017).
[39] B. Dey, N. Quang Hung, D. Pandit, S. Bhattacharya, N. Dinh Dang, L. T. Quynh Huong, D. Mondal, S. Mukhopadhyay, S. Pal, A. De *et al.*, Phys. Lett. B **789**, 634 (2019).
[40] N. Quang Hung, N. Dinh Dang, and L. G. Moretto, Rep. Prog. Phys. **82**, 056301 (2019).